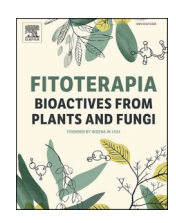
Fitoterapia 185 (2025) 106749



Contents lists available at ScienceDirect

Fitoterapia

journal homepage: www.elsevier.com/locate/fitote





Chemical profiling of *Lycium shawii* via RP-HPLC-QTOF-MS and MS/MS: unveiling its *in-vivo* wound-healing potential supported by molecular docking investigations

Mahmoud Moustafa ^a, Walaa S. Aboelmaaty ^a, Weaam Ebrahim ^a, Reham Hassan Mekky ^b, Mohamed A. Tammam ^c, Amr El-Demerdash ^{d,e,*}, Ahmed M. Zaghloul ^{a,**}

- ^a Department of Pharmacognosy, Faculty of Pharmacy, Mansoura University, Mansoura 35516, Egypt
- b Department of Pharmacognosy, Faculty of Pharmacy, Egyptian Russian University, Badr City, Cairo-Suez Road, 11829 Cairo, Egypt
- ^c Department of Biochemistry, Faculty of Agriculture, Fayoum University, Fayoum 63514, Egypt
- ^d Department of Chemistry, Faculty of Sciences, Mansoura University, Mansoura 35516, Egypt
- e School of Chemistry, Pharmacy and Pharmacology, University of East Anglia, Norwich Research Park, Norwich NR4 7TJ, United Kingdom

ARTICLE INFO

Keywords: Wound-healing Lycium shawii Tandem MS/MS Molecular docking (MDock) Pharmacokinetics

ABSTRACT

Lycium shawii Roem. & Schult., traditionally used across arid regions for treating various ailments, was investigated for its wound-healing potential using integrated metabolomic, computational, and in- vivo approaches. Methanolic extract profiling via RP-HPLC-QTOF-MS/MS identified 62 metabolites, including terpenes, fatty acids, and phenolics. Six key compounds were selected for molecular docking and in silico pharmacokinetic/toxicity analysis, showing strong predicted activity and drug-likeness. In vivo evaluation using a rat excision wound model revealed that treatment with a 2 % extract cream significantly enhanced wound closure (88.63 % by day 14), re-epithelialization, collagen deposition, and VEGF expression compared to controls. The findings suggest that L. shawii promotes wound healing through angiogenesis and tissue regeneration mechanisms. This study supports its traditional use and highlights its pharmaceutical potential.

1. Introduction

The effective management of wounds, particularly those that are extensive and full thickness, continues to pose a significant challenge in

the medical field. Therefore, the search for more effective ways to promote wound repair is an active and crucial area of research for clinicians [1,2]. The development of advanced wound dressings is essential to speed up the healing process and achieve rapid wound closure, avoiding

Abbreviations: ADME/Tox, Absorption, Distribution, Metabolism, Excretion, and Toxicity; AhR, Aryl Hydrocarbon Receptor; AMES, Mutagenicity test (Ames test); ANOVA, Analysis of Variance; AR, Androgen Receptor; ARE, Antioxidant Response Element; ARRIVE, Animal Research: Reporting of In Vivo Experiments; ATAD5, ATPase Family AAA Domain Containing 5; BBB, Blood-Brain Barrier; BPC, Base Peak Chromatogram; Caco-2, Human colon adenocarcinoma cell line; CYP, Cytochrome P450; D0, Day 0 (initial wound day); DBE, Double Bond Equivalence; ER, Estrogen Receptor; GR, Glucocorticoid Receptor; GSK3-β, Glycogen Synthase Kinase 3-beta; H&E, Hematoxylin and Eosin; HIA, Human Intestinal Absorption; HIF, Hypoxia-Inducible Factor; hERG, human Ether-à-go-go-Related Gene; HOB, Human Oral Bioavailability; HSE, Heat Shock Sequence Elements; IHC, Immunohistochemistry; i.p., Intraperitoneal Injection; KEAP1-Nrf2, Kelch-like ECH-associated protein 1 - Nuclear factor erythroid 2-related factor 2; LC-ESI-QTOF, Liquid Chromatography-Electrospray Ionization-Quadrupole Time-of-Flight; LD50, Lethal Dose 50 %; LOAEL, Lowest Observed Adverse Effect Level; MDCK, Madin-Darby Canine Kidney cells; MMP, Mitochondrial Membrane Potential; MS/MS, Tandem Mass Spectrometry; MT, Masson's Trichrome; MU-ACUC, Mansoura University Animal Care Committee; NR, Nuclear Receptor (e.g., AhR, AR, ER, GR, TR); OATP1B1, Organic Anion Transporting Polypeptide 1B1; OCT2, Organic Cation Transporter 2; P-gp, P-glycoprotein; p53, Tumor protein p53; PPAR-gamma, Peroxisome Proliferator-Activated Receptor Gamma; PPB, Plasma Protein Binding; PTEN, Phosphatase and Tensin Homolog; ROS, Reactive Oxygen Species; RP-HPLC-QTOF-MS, Reversed-Phase High-Performance Liquid Chromatography-Quadrupole Time of Flight Mass Spectrometry; RT, Retention Time; SAR, Structure-Activity Relationship; SD, Standard Deviation; SEM, Standard Error of the Mean; SR, Stress Response (e.g., ARE, ATAD5, HSE, MMP, p53); SSVD, Steady State Volume of Distribution; TR, Thyroid Receptor; VEGF, Vascular Endothelial

- * Corresponding author at: Department of Chemistry, Faculty of Sciences, Mansoura University, Mansoura 35516, Egypt.
- ** Corresponding author.

 $\textit{E-mail addresses:} \ a_eldemerdash 83@mans.edu.eg, \ A.Eldemerdash@uea.ac.uk \ (A.\ El-Demerdash), \ amzaghloul@yahoo.com \ (A.M.\ Zaghloul). \ amzagh$

https://doi.org/10.1016/j.fitote.2025.106749

Received 10 April 2025; Received in revised form 9 July 2025; Accepted 19 July 2025 Available online 21 July 2025

0367-326X/© 2025 The Authors. Published by Elsevier B.V. This is an open access article under the CC BY-NC license (http://creativecommons.org/licenses/by-nc/4.0/).

infections caused by pathogenic bacteria remain a major concern, as they can delay the healing process and create substantial public health risks [3]. The body's complex response to wounding involves a carefully coordinated sequence of hemostasis, inflammation, proliferation, and tissue remodeling [4]. These processes depend on the regulated release of signaling molecules from various cell types [5]. Consequently, timely and appropriate wound care is essential for efficient and rapid recovery [6]. The wound care sector provides various products (e.g., Fucidin, MEBO, Calmoseptine, Boroline) and utilizes diverse approaches, spanning traditional herbal methods to contemporary technologies [7]. Herbal remedies are often preferred in developing nations due to affordability, accessibility, perceived efficacy, and fewer side effects [8]. Increasing evidence highlights the medicinal properties of plant-derived compounds in promoting wound repair and treating diseases, offering potential for novel drug development [9,10]. Advances in molecular biology, metabolomics, phytochemical analysis, and drug discovery enable exploration of herbal medicine mechanisms, prominent in systems like Ayurveda and Traditional Chinese Medicine [11-13].

The skin, the body's largest organ, protects against external threats and regulates key functions [14,15]. The skin's layered structure, comprising the epidermis, dermis, and hypodermis [16], predisposes it to injuries that disrupt its integrity and trigger a complex, highly regulated healing cascade [17,18]. However, this process can be compromised by factors such as excessive reactive oxygen species (ROS), infections, or pre-existing health conditions, leading to impaired healing and adverse consequences for patient well-being, healthcare expenditures, and overall productivity [19,20]. This highlights the critical importance of effective wound management strategies aimed at achieving optimal patient outcomes [21].

Medicinal plants represent a crucial source of novel therapeutics globally, with approximately 25 % of medications in developed nations derived from wild plant species [22,23], and continued reliance by tribal communities [24,25]. These plants are integral to traditional medicine for both health maintenance and the development of innovative therapies [26,27], with the World Health Organization estimating that 80 % of developing countries depend on herbal medicines for primary healthcare [28]. Plants produce primary and secondary metabolites, including key phytochemicals like tannins, alkaloids, sugars, terpenoids, steroids, and flavonoids, which are critical to their therapeutic potential [29,30]. With an estimated 300,000 higher plant species on Earth biodiversity supports the vast array of medicinal plants used by billions worldwide with India alone possessing over 8000 critical species [31–33].

The Lycium genus, part of the Solanaceae family, exemplifies this potential, gaining attention for its potent phytochemical compounds and demonstrated antimicrobial, antioxidant, anti-diabetic, anti-inflammatory, anticancer, and other beneficial properties [33-37]. Lycium species are extensively utilized across both culinary and medicinal domains, with their fruits, commonly referred to as goji or wolfberries, having garnered considerable attention as purported "superfoods" [38]. L. shawii Roem. & Schult., also known as Arabian boxthorn or desert thorn, constitutes a perennial plant indigenous to arid environments, characterized by a broad spectrum of traditional medicinal applications. Historically, practitioners throughout disparate geographical regions have employed this species in the treatment of conditions encompassing jaundice, gastrointestinal disturbances, oral lesions, and respiratory ailments [33]. Within the Arabian Peninsula, L. shawii is traditionally administered for the management of dorsalgia, constipation, and pyrexia in livestock, in addition to its sustained application for the amelioration of oral lesions and tussis [39,40].

Scholarly investigations have elucidated a constellation of pharmacological attributes inherent to *L. shawii*, including antidiabetic [37], hypotensive [41], and antiplasmodial activities [42]. Furthermore, extracts derived from *L. shawii* have demonstrated antitrypanosomal, antiinflammatory, hepatoprotective, hypoglycemic, and cytotoxic effects [37,39]. Despite prior research on the phytochemical composition and pharmacological effects of *L. shawii* [33,43], a comprehensive chemical characterization of its complex extract remained incomplete. To address this, the present study conducted a thorough metabolic profiling of *L. shawii* methanolic extract using RP-HPLC-QTOF-MS and MS/MS, revealing 62 diverse secondary metabolites, primarily terpenes (24) and fatty acids/long-chain amides (27), along with organic acids, phenolic compounds, and other constituents.

Given the increasing interest in natural products for wound healing due to their efficacy and perceived safety, and the need for rigorous investigation the therapeutic potential of *L. shawii* methanolic extract in facilitating wound repair was explored [44]. In vivo experiments were conducted to assess wound closure, followed by histopathological assessments to understand tissue remodeling. Immunohistochemical analyses were also performed to delineate the role of VEGF in angiogenesis [44,45]. By integrating *in-silico* simulations and in vivo findings, a robust understanding of the biological and molecular mechanisms governing the wound-healing attributes of the *L. shawii* methanolic extract was achieved.

2. Materials and methods

2.1. Plant material

Aerial parts (leaves and stems) of *L. shawii* were collected from Saint Catherine, South Sinai, Egypt (coordinates: 28.5558° N, 33.9514° E) in March 2024. The taxonomical features were kindly confirmed by Prof. Dr. Ibrahim Mashaly, Department of Botany, Faculty of Sciences, Mansoura University, Egypt. A voucher specimen has been deposited in the Department of Pharmacognosy, Faculty of Pharmacy, Mansoura University (MAWW 010320). The airdried leaves and stems (500 g) were powdered in an electric mill and then extensively extracted with MeOH at room temperature, to afford after evaporation of the solvents in vacuo a crude extract (20.30 g).

2.2. In vivo examination of L. shawii extract wound healing properties

2.2.1. Experimental animals

Fifteen-Dawley male adult rats (200 \pm 20 g) were housed under standard conditions of animal care, ambient temperature, and steady light/dark cycles, with free access to water and standard animal food during the experiment. The animals were prepared for wound excision induction by intraperitoneal injection (i.p.) of ketamine (5 mg/kg) and xylazine (5 mg/kg). The dorsal fur was carefully removed with scissors and razors to expose the underlying skin. Following the disinfection with 70 % alcohol wipes, a uniform circular cap with a diameter of 2.5 cm was used to trace the designated area of the skin, which was carefully excised, sparing the muscle layer [46]. Animals were returned to the cages, and the day was set as (D0). All procedures and treatment were approved by Mansoura University Animal Care Committee (MU-ACUC), Mansoura University, Mansoura, Egypt (Ethical Approval Code: 34-2025 (PHARM.PhD.24.12.47), and following the "Principles of Laboratory Animal Care, National Materials Institute of Health Publication revised 1985" and ARRIVE guidelines for experimental research.

2.2.2. Preparation of topical formulations

The topical formulation of L. shawii was prepared at a concentration of 2 % (w/w). Briefly, the required amount of the methanolic crude extract was incorporated into a simple oil-in-water cream base (Simple Cream BP) using geometric dilution. The mixture was triturated thoroughly until a smooth, homogenous cream was obtained. The positive control formulation (Fucidin cream®) was used directly from its commercial packaging. All formulations were prepared fresh before the initiation of the study to ensure stability.

2.2.3. Experimental study design (experiment ran for two weeks)

On the next day (D1), the animals were randomly divided into 3

subsequent groups (n=5). Group 1 (Positive control): the wound was left untreated. Group 2 (L.s methanolic extract): the animals were treated with L. shawii methanolic extract (2 % w/w in cream base). Group 3 (Fucidin cream®): the animals were treated with Fucidin cream® (Fuscidic acid, 2 % w/w). Animals of group 2 and 3 were treated once daily with the designated treatment for 14 days (Topically, 0.5 g /animal). The dorsal wounds were photographed on days 0, 3, 9 and 14.

2.2.4. Tissue samples collection

On Day 14, the animals were euthanized with a ketamine injection (5 mg/kg, i.p.) and xylazine (5 mg/kg, i.p.). Their fur was trimmed to expose the wound area to be photographed before collecting the wounded skin samples, which were preserved in 10 % neutral buffered formalin. Also, a section of normal skin was exercised from the unaffected area and prepared as mentioned above for comparative purposes and to serve as a negative control. Using ImageJ, wound contraction (%) was calculated by measuring wound area (cm²) at days 3, 9, and 14 (Dn) to be compared with the initial wound area (cm²) at D0 according to the following equation [47].

Wound contraction (%) = ((wound area at D0 – wound area at Dn) /(wound area at D0)) \times 100

and the statistical analysis was performed using a two-way ANOVA, followed by Tukey's post hoc test. These analyses were conducted using GraphPad Prism software version 8.3.0 (San Diego, CA, USA). Results are presented as the mean \pm standard deviation (SD) of five rats. A *p*-value of <0.0001 was used to determine statistical significance, and the difference was documented as significant.

2.2.5. Histopathological and immunohistochemical examination

Histopathological changes within the wound area were assessed on day 14, where preserved skin samples of the examined groups were embedded in paraffin and cut into 4 μ m-thick coded sections, using hematoxylin and eosin (H&E) and Masson's trichrome (MT) staining to evaluate the collagen fiber deposition in the dermal layer, followed by the detection of histological alterations via representative images from the examined groups at both low (X100) and high (X400) magnifications using an Olympus® digital camera connected to an Olympus® light microscope (Shinjuku Co., Tokyo, Japan).

2.2.6. Immunohistochemical examination

Another section set of the preserved skin samples was deparaffinized and treated with an immunohistochemistry (IHC) staining kit (InvitrogenTM, Ca., USA), following the manufacturer's protocol. Briefly, the sections were incubated overnight with vascular endothelial growth factor (VEGF) primary antibody (ABclonal Co., Woburn, USA, dilution 1:500). Then, they were incubated with horseradish peroxidase-conjugated secondary antibodies, visualized by 3,3'-diaminobenzidine tetrahydrochloride (Genemed, Biotechnologies Inc., USA), and finally counterstained with Mayer's hematoxylin to be examined at both low (X100) and high (X400) magnifications. Using ImageJ software version K 1.45, the stained area of VEGF (%) was measured using five randomly taken non-overlapping fields, and the values presented as mean \pm standard error of the mean (SEM).

2.3. Metabolic profiling

2.3.1. Chemicals and reagents

Fisher Chemicals (HPLC-MS grade) (ThermoFisher, Waltham, MA, USA) supplied methanol, acetonitrile, and glacial acetic acid. A Milli-Q system (Millipore, Bedford, MA, USA) produced ultrapure water.

2.3.2. Analysis by RP-HPLC-ESI-QTOF-MS and -MS/MS

Reversed-phase high-performance liquid chromatography (RP-HPLC) was done using an Agilent 1200 series rapid resolution analyzer

(Agilent Technologies, Santa Clara, CA, USA) with a G7104C quaternary pump and G7129A autosampler. Separation was done using a Poroshell 120 HiLiC Plus (150 mm \times 3 mm, 2.7 μm particle size, Agilent Technologies). The system was connected to a 6530-quadruple time of flight (Q-TOF) LC/MS (Agilent Technologies) with dual ESI interface [48,49]. Metabolite characterization and data analysis were done on MassHunter Qualitative Analysis B.06.00 (Agilent Technologies) [50,51]. Conditional formatting and bubble plot were performed by Microsoft Excel 365 (Redmond, WA, USA) and Minitab 17 (Minitab, Inc., USA), respectively.

2.4. Preparation of the protein structures and molecular docking (MDock)

To assess the potential of L. shawii metabolites for activity and to give insights into the structure-activity relationships of the selected compounds, a virtual screening protocol was employed, integrating molecular docking and in silico prediction of activity. Initially, 62 compounds identified in L. shawii extract via RP-HPLC-MS and tandem MS/MS were subjected to a virtual screen against key wound healing targets: GSK3-β, HIF Hydroxylase, KEAP1-Nrf2 complex, and PTEN. Based on the virtual screening results, the six compounds exhibiting the best affinity (as determined by optimal docking poses) against the active sites of these targets were selected for further molecular docking. For molecular docking (MDock), the structures of the target proteins (PDB codes: 6ae3, 5a3u, 6qmc and 6w30) were prepared by removing water molecules and unnecessary molecules, correcting crystallographic disorders and unfilled valence atoms, minimizing energies, and saving as PDBQTP files. The 2D structure of each of the six selected compounds was drawn using Chem-Bio Draw Ultra16.0, saved as an SDF file, protonated, subjected to energy minimization, and saved as PDBQTP files. The prepared ligands were then docked against the target proteins using Autodock Vina 1.5.7 software [52] with a rigid receptor and flexible ligands. During docking refinement, each molecule was allowed to generate twenty different poses, and the resulting docking scores (affinity energy) of the best-fitted poses were recorded. 3D and 2D figures were generated using Discovery Studio 2024 visualizer [53].

2.5. Physicochemical properties, pharmacokinetic and toxicity profiles and in silico prediction

To assess the potential of *L. shawii* examined metabolites for pharmaceutical development and druggability, in silico prediction of physicochemical, pharmacokinetic, and toxicity profiles of these six selected compounds were calculated using the Deep-PK online web tool (https://biosig.lab.uq.edu.au/deeppk/, accessed on [on 25 February 2025]) [54]. This tool encompasses nine general properties: boiling point (°C), hydration free energy (which indicates the drug's aqueous solubility), log D7.4 (the logarithm of the n-octanol/water distribution coefficient, representing the lipophilicity of a molecule at pH 7.4), log P (the logarithm of the n-octanol/water distribution coefficient), log S (the logarithm of aqueous solubility at a temperature of 20–25 °C), log VP (the logarithm of the vapor pressure, representing the volatility of a molecule at 25 °C), melting point (°C), pKa acid, and pka basic (which control its pharmacokinetic properties).

Seven absorption properties (Caco-2 permeability, Human oral bioavailability, Human intestinal absorption (HIA), Madin-Darby Canine Kidney cells (MDCK) permeability, skin permeability, P-glycoprotein substrate, P-glycoprotein I inhibitor), four distribution properties (BBB (blood-brain barrier) permeability, fraction unbound (human), Plasma protein binding (PPB), Steady State Volume of Distribution (SSVD)), seven metabolism properties (CYP2D6 substrate, CYP3A4 substrate, CYP1A2 inhibitor, CYP2C19 inhibitor, CYP2C9 inhibitor, CYP2D6 inhibitor, CYP3A4 inhibitor), and three excretion properties (total clearance, Half-life, renal OCT2 substrate) were available through the Deep-PK tool. The 33 available toxicity properties (AMES

mutagenesis, avian toxicity, honey bee toxicity, bioconcentration factor, biodegradation, carcinogenicity, crustacean toxicity, liver injury I, liver injury II, eye corrosion and irritation, maximum tolerated dose (human), hERG inhibitor, Daphnia magna toxicity, micronucleus formation, NR-Aryl hydrocarbon Receptor (AhR), NR-Androgen Receptor (AR), NR-Androgen Receptor (AR) Ligand-Binding Domain (LBD) activation, NR-aromatase inhibition, NR-Estrogen Receptor (ER), NR-Estrogen Receptor (ER) Ligand-Binding Domain (LBD), NR-Glucocorticoid Receptor (GR), NR-Peroxisome Proliferator-Activated Receptor Gamma (PPARgamma), NR-Thyroid Receptor (TR), oral rat acute toxicity (LD50), oral rat chronic toxicity (LOAEL), Fathead Minnow toxicity, respiratory disease, skin sensitization, SR-Antioxidant Responsive Element (ARE), SR-ATAD5 (ATPase Family AAA Domain Containing 5) gene, SR-Heat Shock Sequence (HSE) elements, SR-Mitochondrial Membrane Potential (MMP), and SR-p53 pathway) in Deep-PK were calculated to predict the potential toxicity profiles of these compounds.

3. Results and discussion

3.1. In vivo examination of L. shawii extract wound healing properties

3.1.1. Wound area and wound contraction (%) estimation

A wound is defined as a disruption in the anatomical integrity of any biological tissue, induced by physical, mechanical, chemical, or microbial agents. The subsequent wound healing process is a complex biological cascade that serves to restore the structural and functional integrity of injured or damaged tissues. This process is generally characterized by four sequential, yet overlapping phases: coagulation and hemostasis, inflammation, proliferation, and the final remodeling phase of scar tissue formation, or maturation [44]. Herbal medicines are a significant component of primary healthcare provision in many resource-limited nations globally. The establishment of scientific evidence supporting their efficacy is critical, not only to encourage adoption within formal healthcare systems but also to ensure consumer safety [55]. Therefore, this study investigated the wound-healing activity of *L. shawii* aerial parts methanolic extract. We employed RP-HPLC-QTOF-MS and MS/MS techniques to profile its chemical constituents.

These analytical findings were further corroborated by molecular

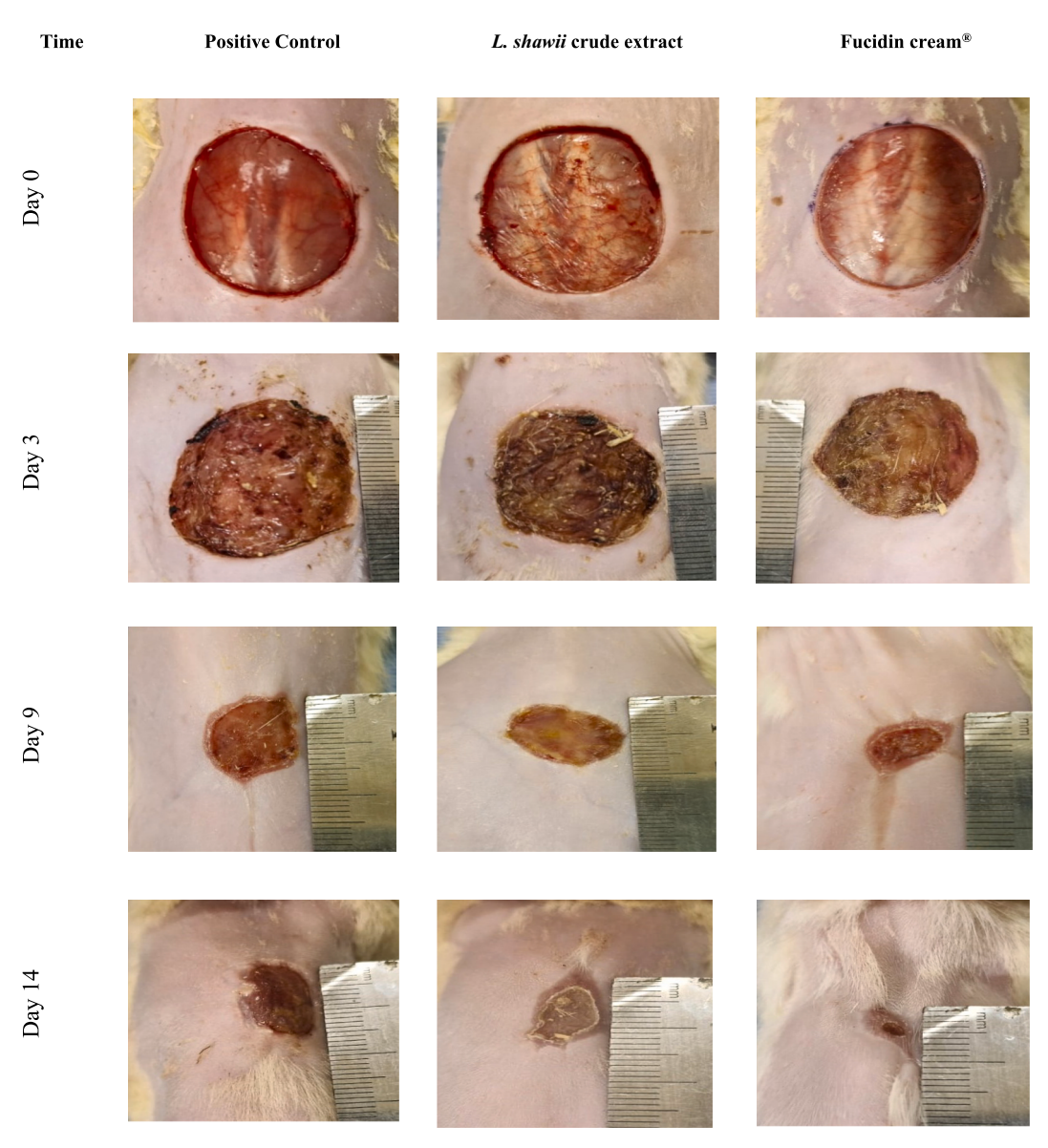


Fig. 1. Macroscopic images of wound closure over a 14-day healing period in positive control, crude extract, and Fucidin-treated groups.

wound over the docking investigations to elucidate the underlying mechanisms of action. The visual assessment of wound closure was a key component of our in-vivo study. Fig. 1 presents photographic evidence of the wound areas on the dorsal skin of the subjects, demonstrating the healing process in the positive control (untreated) group, those treated with the *L. shawii* methanolic crude extract (Total Extract), and those treated with Fucidin cream® (Fuscidic acid 2 %) at days 0, 3, 9, and 14 (Fig. 1).

This in vivo study investigated the wound-healing potential of the *L. shawii* extract by evaluating wound contraction over a 14-day period in a rat model. The extract's performance was compared to that of a control group and the standard wound-healing agent, Fucidin cream®. The results are presented as wound area (cm 2 ± SD) in Fig. 2.a, and wound contraction percentages (% ± SD) in Fig. 2. b.

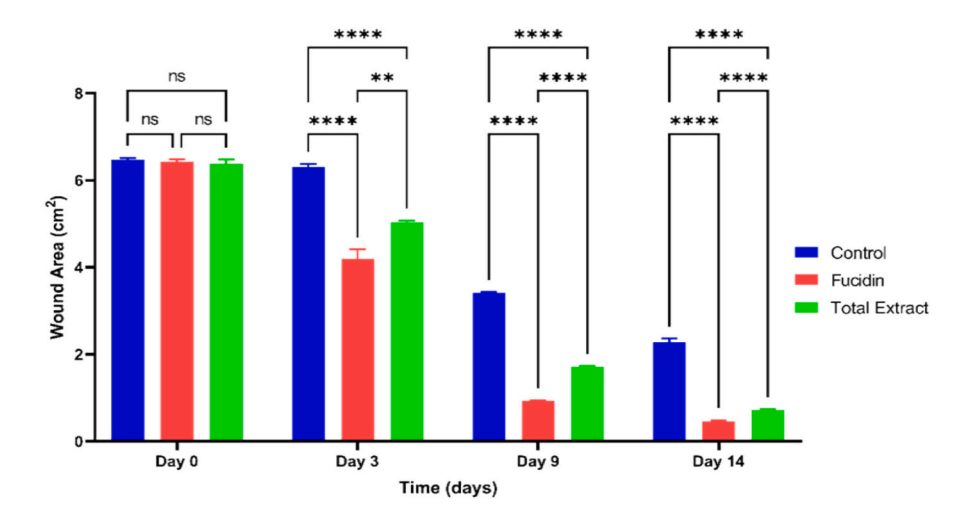
Where Fig. 2a shows that the initial wound areas on day 0 were similar across all groups. Over the course of the 14-day study period, all groups demonstrated a progressive reduction in wound area. Fucidin showed the fastest rate of reduction, but it is important to note that the extract demonstrated a significantly more pronounced reduction compared to the control in each time point and demonstrated promising results in reducing the wound area.

By day 14, the control group exhibited a substantial reduction with a wound area of $2.285 \pm 0.080 \text{ cm}^2$, while the Fucidin group exhibited a markedly lower wound area $(0.460 \pm 0.029 \text{ cm}^2)$. Notably, the extract

b

demonstrated a reduction to $0.725\pm0.011~cm^2$ at the end of the study, indicating a considerable reduction compared to the control and a promising healing effect. Additionally, Fig. 2b displays the calculated wound contraction data for each group across the 14-day study. On day 3, while the Fucidin group demonstrated the highest contraction rate (34.556 \pm 3.820 %), the extract group showed a considerable contraction of 21.114 \pm 1.419 %, which is significantly better than the control (2.638 \pm 0.597 %). By Day 9, Fucidin exhibited the most pronounced mean wound contraction (85.436 \pm 0.079 %). While the extract exhibited a lower contraction compared to Fucidin, it still showed a very significant and much higher wound contraction (73.113 \pm 0.590 %) compared to the control (47.303 \pm 0.254 %). By day 14, while Fucidin showed the highest mean wound contraction (92.832 \pm 0.509 %), the extract still showed a considerable contraction (88.633 \pm 0.331 %) at the end of the study.

In comparison with previous studies, our findings on wound area reduction and wound contraction in the *L. shawii* extract-treated group are highly encouraging and consistent with reports on other *Lycium* species. For instance, research on *Lycium barbarum* has demonstrated that its polysaccharides enhance fibroblast proliferation, collagen deposition, and angiogenesis, thereby accelerating wound closure and improving collagen maturation [56–58]. These similarities suggest that the bioactive compounds in *L. shawii* may function through comparable regenerative mechanisms, such as upregulating vascular endothelial



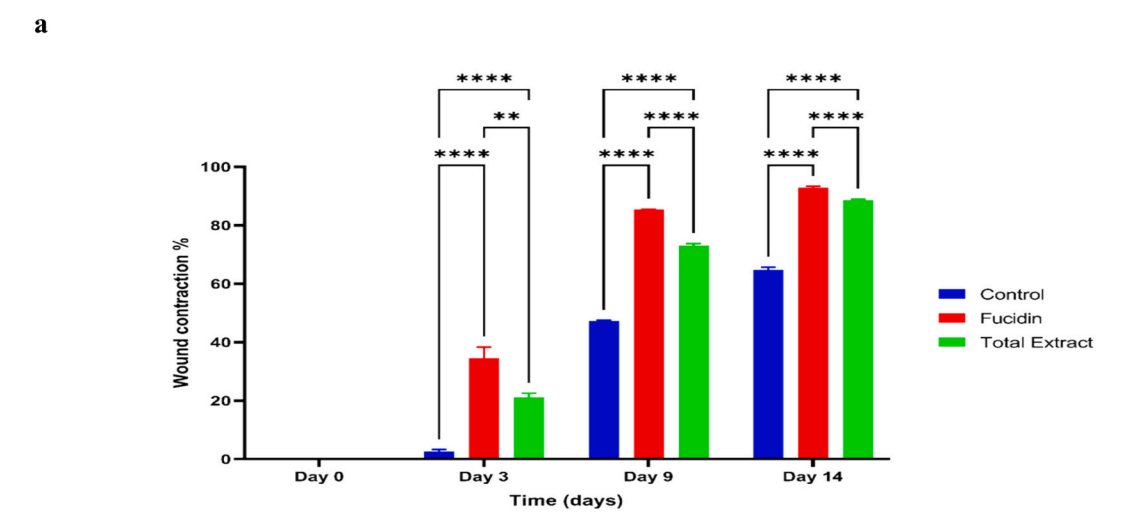


Fig. 2. a) Wound area (cm²) changes across treatment groups over a 14-day period, b) Wound contraction (%) in control, Fucidin, and Total Extract groups over a 14-day healing period.

growth factor (VEGF) and modulating inflammatory cytokines, which are vital for effective tissue repair. The significant reduction in wound area observed in our experiment further underscores the therapeutic potential of L. shawii. This outcome is consistent with studies highlighting that herbal formulations rich in polyphenols and flavonoids significantly decrease wound size by promoting rapid reepithelialization and reducing inflammation [59,60]. The alignment between our wound contraction data and these earlier studies emphasizes the efficacy of L. shawii extract in facilitating tissue regeneration, potentially through similar biochemical pathways. These comparative insights not only validate our observations but also highlight the promise of L. shawii as a natural therapeutic agent in wound management. Overall, the consistency of our results with previous studies provides a robust foundation for further investigations into the molecular mechanisms underlying L. shawii's wound-healing properties and supports its potential for future clinical applications.

3.1.2. Histopathological examination

In contrast to, the microscopic examination of H&E-stained skin sections obtained from the standard normal skin revealed a normal epidermal structure (e) with an underlying dermis (d) exhibiting typical connective tissue organization and skin appendages, the examined sections from the positive control group demonstrated a notable ulcerated wound area (W) filled with inflamed granulation tissue. This tissue was characterized by the presence of capillary buds (red arrows), young fibroblasts, and a high number of inflammatory cells (black arrows), predominantly neutrophils and some macrophages. Furthermore, the extract group displayed incomplete re-epithelization (e), with several non-keratinized epithelial layers overlying an inflamed granulation tissue (W). This tissue exhibited fewer inflammatory cells (black arrows), and capillary buds (red arrows) compared to the positive control group. Notably, the Fucidin group showed complete re-epithelization (e), with a thicker, keratinized epithelial layer. The underlying tissue (W) in this group consisted of mature vascular connective tissue, which showed less inflammatory cells and had a few macrophages (black arrows) than the other groups and prominent capillary buds (red arrows), which clearly distinguishes it from both the positive control and extract groups (Fig. 3a and Fig. S1a).

Collagen is an abundant protein in the connective tissues that plays a crucial role in wound healing [61]. MT-stained sections obtained from the normal skin displayed a typical epidermal structure (e) overlying a dermis (d) characterized by dense, bluish collagen. In contrast, sections from the positive control group exhibited an ulcerated wound area (W) containing loosely arranged, faint blue collagen (black arrows). Notably, both the extract and Fucidin groups showed a marked increase in collagen deposition compared to the positive control group. Specifically,

the extract group revealed a wound area (W) with an increased deposition of bluish collagen (black arrows), indicative of collagen formation during wound healing and tissue repair. The Fucidin group, on the other hand, demonstrated a wound area (W) with a denser deposition of bluish collagen (black arrows), suggesting a more advanced stage of collagen maturation compared to both the positive control and extract groups (Fig. 3b and S1b).

3.1.3. Immunohistochemical examination

To assess the expression of vascular endothelial growth factor (VEGF) within the wound area on day 14, immunohistochemical (IHC) analysis was conducted. Where, microscopic examination of immunostained normal skin sections revealed few positively brown-stained endothelial cells (black arrows) within the dermis (d). In contrast, wounded skin sections from both the positive control and extract groups showed an increased number of positively brown-stained endothelial cells (black arrows) within the wound area (W), suggesting an increase in angiogenesis. The Fucidin cream® group, however, exhibited the highest number of positively brown-stained endothelial cells (black arrows) in the wound area (W), which suggests a more pronounced neovascularization compared to all other groups (Fig. 4 and S2).

Furthermore, quantitative analysis of VEGF staining demonstrated a significantly higher VEGF-stained area in the extract group (31.00 \pm 1.871 %) compared to negative control group (7.000 \pm 0.9487 %) (p < 0.0001). While the Fucidin cream® group exhibited a more pronounced, statistically significant increase in VEGF staining (40.00 \pm 1.581 %) compared to the control normal group (p < 0.0001), Control Positive (21.00 \pm 1.871 %), and the Extract groups (p < 0.0001) (Fig. 5).

This finding, alongside the observation that Fucidin cream® also caused an increase in VEGF, demonstrates that both the *L. shawii* extract and Fucidin cream® induce angiogenesis in the wound area through their effects on VEGF production. The process of angiogenesis, a hallmark of effective wound repair, involves the formation of new blood vessels from existing ones. This regeneration is critical as it facilitates the transport of oxygen and nutrients to the wound site while enabling the removal of metabolic waste products [62]. Vascular endothelial growth factor (VEGF) is a key regulator of angiogenesis, widely recognized as the most dynamic and essential growth factor involved in this process [63]. Furthermore, it has been reported that VEGF plays a significant role in mitigating skin injuries through the activation and recruitment of endothelial progenitor cells derived from the bone marrow [64].

Although the Fucidin® cream showed a faster rate of wound contraction, the significant healing efficacy of *L. shawii* extract is highly relevant due to its distinct, multi-targeted mechanism. Unlike the singular antimicrobial action of Fucidin®, our extract acts as a complex

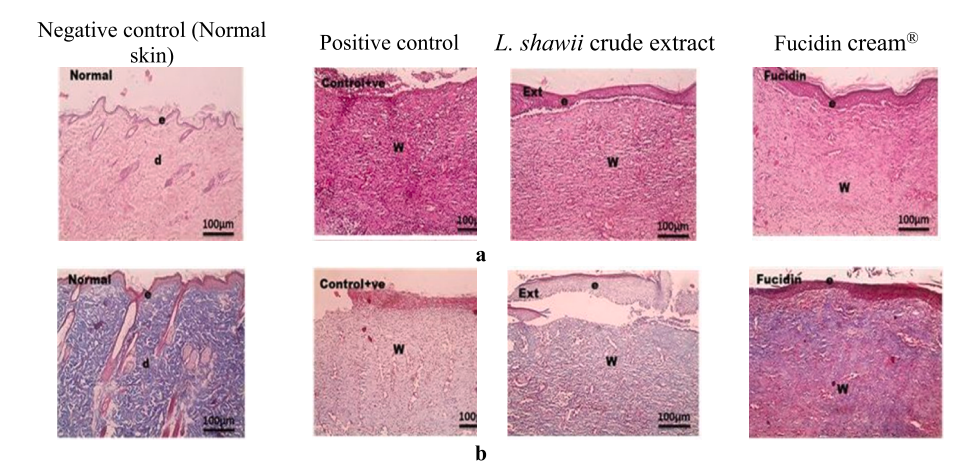


Fig. 3. Histological analysis of wound tissue on Day 14, magnifications: X100 (bar: 100 μm), a) stained with hematoxylin and eosin (H&E). b) Collagen deposition in wound tissue shown by Masson. e: epidermis; d: dermis and w: wound.

Fig. 4. VEGF expression in wound tissue on Day 14, determined by immunohistochemistry (IHC). Magnifications: X100 (bar: 100 μm). e: epidermis; d: dermis and w: wound.

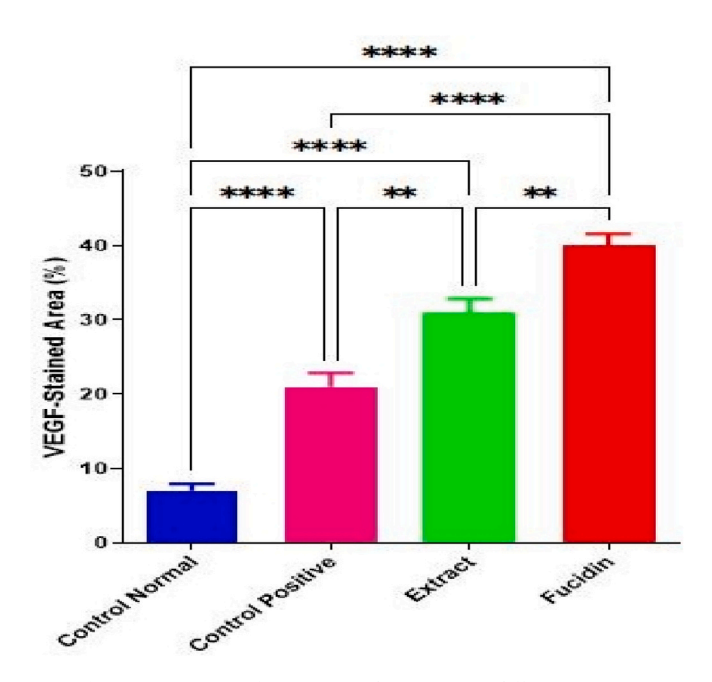


Fig. 5. Percentage of VEGF-stained areas across different groups.

mixture of phytochemicals that simultaneously promotes angiogenesis, modulates inflammation, and supports tissue regeneration, as evidenced by our histopathological findings. This holistic, pro-regenerative approach offers potential synergistic effects and may reduce the risk of antimicrobial resistance. Therefore, while not outperforming the pure compound standard in this model, *L. shawii* extract is established as a compelling candidate for development as a safe and effective natural therapeutic alternative.

This pro-regenerative capacity is consistent with the extract's rich phytochemical profile. For instance, its triterpenoids represent the same pharmacologically active scaffolds found in renowned wound-healing botanicals like *Centella asiatica* and *Calendula officinalis* [65,66], while its unsaturated fatty acids provide crucial inflammation-attenuating effects, a therapeutic principle also leveraged by established remedies like rosehip oil [67]. Moreover, this chemical profile, dominated by lipophilic compounds, also distinguishes *L. shawii* from its more famous relative, *L. barbarum* (goji berry), whose therapeutic effects are often linked to its high content of water-soluble polysaccharides. This distinct chemistry underscores the diverse therapeutic potential within the *Lycium* genus and highlights the value of investigating its lesser-known species.

3.2. Metabolic profiling

The metabolic profiling of *L. shawii* Roem. & Schult. aerial parts extract employing RP-HPLC-MS and tandem MS/MS in both negative and positive ionization modes revealed the presence of 62 metabolites (Chart 1).

In this sense, Fig. 6a shows the extract's base peak chromatogram. The metabolite characterization strategy was based on earlier investigations [65,66] taking into consideration the generated molecular formulae, retention times (RT), double bond equivalence (DBE), molecular ion peaks (m/z), neutral losses, and peak areas (Fig. 6b) consulting relevant literature and databases [67–71]. The annotated metabolites were grouped into terpenes (24), fatty acids and long-chain amides (27), organic acids (3), phenolic compounds, lactones, furans, and ketones (Fig. 6b and S3-S5, 2 Table 1).

The occurrence of terpenes was widely noticed, with 24 derivatives being categorized into monoterpenes, sesquiterpenes, and triterpenes. In this sense, monoterpenes were noticed as two isomers of loliolide I-II (peaks 1, 2) as monoterpene lactones (Fig. S7a) as well as β -methylionone (peak 49). It bears noting that they were mentioned in *Solanum lyratum* and *Soalnum lycopersicum*, in a respective manner [67,68].

Concerning sesquiterpenes, they were the most abundant class of terpenoid derivatives, with 19 derivatives. They were classified as eudesmane sesquiterpenes, vetispirane sesquiterpenes, and sesquiterpene saponins. As for eudesmane sesquiterpenes, two isomers of lyciiterpenoid A/B (peaks 17, 20) (Fig. S7b) were observed being characterized before in L. chinense. Furthermore, five isomers of lyciiterpenoid C/(2S)-2-(2-hydroxypropan-2-yl)-5,8-dimethyl-1,2,3,4-tetrahydronaphthalen-2-ol (peaks 6, 13, 14,21,33) were observed (Fig. S7c) in agreement with previous study on L. chinense [68,69]. Vetispirane sesquiterpenes were annotated as (+)-anhydro- β -rotunol I-II (peaks 10, 36) (Fig. S8a), 2-hydroxysolajiangxin E/7-hydroxylsolajiangxin I (peak 12) (Fig. S8b), and solavetivone I-II (peaks 50, 51) (Fig. S8c) that were noticed before in Solanum lyratum [68,71,72]. Additionally, sesquiterpene saponins were detected as pyishiauoside Ib I-II (peaks 9, 11) (Fig. S9a), mukurozioside Ib I-IV (peaks 15, 16, 18, 22) (Fig. S9b), and mukurozioside Ia (peak 19) (Fig. S9c) exhibiting the sequential loss of hexose moieties (162 Da) and/or deoxyhexose moieties (146 Da) as well as n CHOH moieties (n × 30 Da). This is the first report of these sesquiterpene saponins in the family Solanaceae. Whereas they were mentioned in Sapindus mukorossi, Sapindaceae [73]. Regarding triterpenoids, two isomers of the limonoid salannin (peaks 23, 25) were noticed as the first report in Solanaceae [68].

With regards to fatty acids and long-chain amides, 27 derivatives were noticed exhibiting dehydration and/or decarboxylation [66,74]. They were sub-grouped into saturated fatty acids (5), monounsaturated fatty acids (4), diunsaturated fatty acids (11), polyunsaturated fatty acids (5), and two long-chain amides. In this context, lauric acid (peak 48), myristic acid (peak 53), palmitic acid (peak 58) and two isomers of stearic acids (peaks 61, 62) (Fig. S10a) were noticed as examples of saturated fatty acids. It bears noting that they were described for the first time in the genus Lycium. However, they were described in Solanaceae in Mandragora autumnalis, Hyoscyamus niger, and Solanum chacoense (Table 1, Fig. S4) [67,68]. Moreover, monounsaturated fatty acids were detected as ricinoleic acid I-II (peaks 41, 45) and oleic acid I-II (peaks 59, 60), which were described before in Solanum dulcamara and Nicotiana tabacum, Solanaceae [68], respectively. Linoleic acid I-II (peaks 56, 57), (S)-coriolic acid I-III (peaks 32, 34, 35) (Fig. S10b), and 9-oxo-10E,12(Z/ E)-octadecadienoic acid I-VI (peaks 26, 28, 30, 38, 40, 42) were noticed in Lycium for the first time and represented diunsaturated fatty acids

Chart 1. A list of 62 identified metabolites in L. shawii leaf extract.

where they were mentioned before in *Deprea subtriflora, Nioctiana tabacum*, and *Capsicum annuum*, Solanaceae, respectively [68] (Table 1, Fig. S4). Linolenic acid (peak 52) and colnelenic acid (peak 31) were annotated in *L. shawii* extract, portraying polyunsaturated fatty acids that were mentioned before in *Withania somnifera* and *Solanum tuberosum* (Solanaceae) [68]. Besides, three isomers of stearidonic acid (peaks 24, 27, 29) (Fig. S10c) were characterized where they were mentioned for the first time in the family Solanaceae, where they were described in *Vincetoxicum funebre*, Apocyanaceae [68] (Table 1, Fig. S4). As for long-chain amides, palmitamide and (peak 54) *N*-methylpalmitamide (peak 55) were mentioned for the first time in the family Solanaceae but were observed in *Boronia koniambiensis* (Rutaceae) and *Gossypium hirsutum* (Malvaceae) [68], (Table 1, Fig. S4).

Three organic acids were observed as 4,4-dimethylheptanedioic acid (peak 3), Dibutyl phthalate I-II (peaks 44, 47) (Fig. S11a) that were mentioned in Solanum melongena and L. barbarum, respectively [68]. With respect to phenolic compounds, three flavone isomers of 8-(2hydroxypropan-2-yl)-5-hydroxy-7-methoxy-6-methyl-4'-methoxyflavone (peaks 4, 5, 7) (Fig. S11b) stated previously in Nioctiana tabacum, Solanaceae [68]. In addition, the phenols were characterized doitungbiphenyl A I-II (peaks 43, 46) (Fig. S8c) in agreement with their previous description in Nioctiana tabacum, Solanaceae [68]. The α - β -unsaturatedy-lactone (-)-hydroxydihydrobovolide (peak 8) was observed which was mentioned earlier in Solanum nigrum, Solanaceae [68]. Moreover, the cyclohexanone blumenol (peak 37) A was observed, as stated earlier in Lycium barbarum [70]. In regard to isobenzofurans, 2,2-Dimethyl-6,8-dihydro-2H-furo[3,4-g]chromene (peak 39) was noticed and mentioned previously in Nioctiana tabacum, Solanaceae [68], (Table 1, Fig. S5).

3.3. Molecular docking (MDock), binding energies studies and structure-activity relationships (SARs) analysis

To elucidate the molecular mechanisms underpinning the observed wound-healing properties of *L. shawii* extract, molecular docking studies were performed to explore the potential of *L. shawii* metabolites to interact with key regulatory proteins involved in angiogenesis and wound repair. Following an initial screening of the 62 compounds identified in *L. shawii* extract through RP-HPLC-QTOF-MS and MS/MS, six metabolites (2-hydroxysolajiangxin-E, Salannin I-II, Doitungbiphenyl-A I-II, Lyciiterpenoid C I-V, Lyciiterpenoid-A, Blumenol-A), (Fig. S4 and S5) were selected for more in-depth docking studies due to their excellent predicted binding affinity for the chosen target proteins.

These docking studies also provide insight into the binding energies and potential structure-activity relationships (SARs) of these metabolites. The target proteins, GSK3- β [75], HIF Hydroxylase [76,77], KEAP1-Nrf2 complex [76–78], and PTEN [79,80], were selected due to their established roles in driving VEGF expression and the subsequent angiogenesis essential for effective wound closure. To ensure the reliability of the docking protocol, the co-crystalized ligands for each target protein were also docked into their respective binding sites (Table 2). The findings of these docking studies provide insight into the possible mechanisms through which *L. shawii* extracts might exert their observed wound-healing properties.

Salannin I-II demonstrated the highest affinity for GSK3- β . This favorable interaction was mediated by seven hydrophobic π -Alkyl interactions with residues in the active site (Val70, Leu132, Vall10, Cys85, Ala83) and four hydrogen bonds (Lys85, Cys199, Tyr134, and Arg141 with distances of 2.42, 3.08, 3.01, and 2.91 Å) (Fig. 7), resulting in a

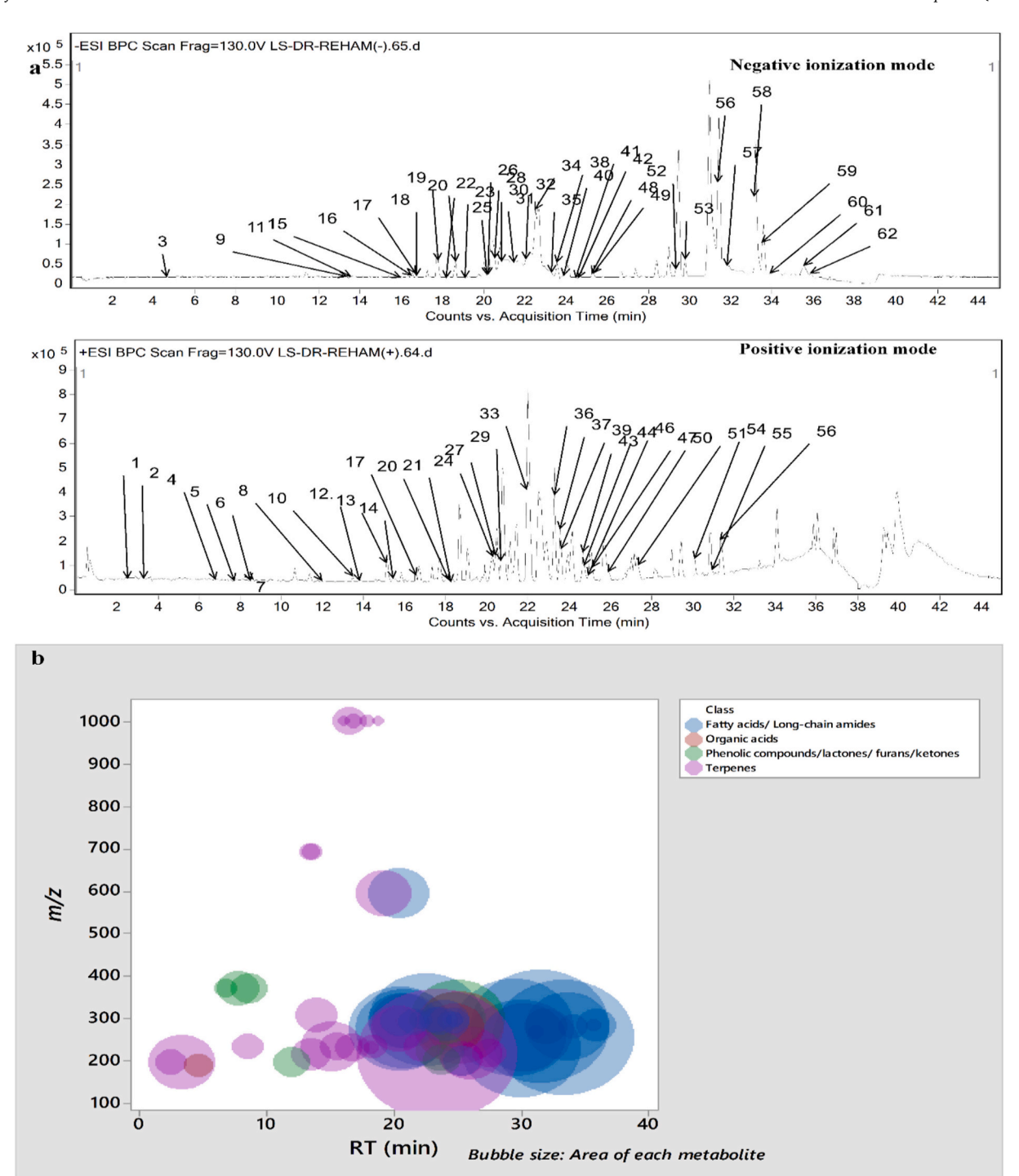


Fig. 6. (a) Base peak chromatograms (BPCs) of the L. shawii leaf extract in negative and positive ionization modes, (b) bubble plot of observed masses (m/z) versus retention time for metabolite classes and peak areas.

strong binding energy (-9.45 kcal/mol). This strong binding suggests that salannin I-II may act as a GSK3- β inhibitor. GSK3- β negatively regulates the Nrf2 pathway; therefore, the potential for salannin I-II to modulate its activity is significant. This modulation of GSK3- β leads to Nrf2 activation, increasing VEGF expression and enhanced angiogenesis, thereby promoting wound healing [75]. Furthermore, the binding affinity of salannin I-II compares favorably to the co-crystalized ligand Morin (-7.11 kcal/mol) which exhibited six hydrophobic π - π interactions and five hydrogen bonds with Val110, Leu132, Cys199, Leu188, Ala83, Val70, Asp133, Lys85, Asp200, and Asn64 with distances of 1.91, 2.93, 2.37, 2.96, and 2.39 Å, respectively (Fig. 8).

The high binding energy observed for salannin I-II, and the involvement of hydrogen bonds suggest that the ester groups, and the decalin ring system are key determinants of high binding energy. These groups likely enable the observed formation of hydrogen bonds with Lys85, Cys199, Tyr134, and Arg141 in the GSK3- β active site. Doitungbiphenyl A I-II also exhibited a notable binding affinity for GSK3- β (-7.02 kcal/mol). The interactions were characterized by ten hydrophobic π -sigma, π -sulfur, and π -Alkyl interactions with Ile62, Val70, Lys85, Ala83, Leu188, Val110, Leu132, Cys199, and Phe67, alongside two hydrogen bonds with Val135, and Asp133 with distances of 2.54, and 2.54 Å, (Fig. 9). This suggests that even in the absence of the ester

 Table 1

 A list of 62 Metabolites characterized in L. shawii.

					je					S							
Peak No	RT (min)	[M-H]-	[M+H+]	×	Ionization Mode	Molecular formula	Score	Епог (ррт)	Error (mDa)	Main fragments	DBE	Proposed	Subclass	Species	Family	Area	%
1	2.45		197.1167	196.104 4	P	C ₁₁ H ₁₆ O ₃	74.4	0.2	0.4	N.D.	4	Loliolide I	Monoterpene lactone	Solanum lyratum	Solanaceae	1.92E+05	0.40
2	3.32		197.1165	196.104 4	P	C ₁₁ H ₁₆ O ₃	94.2	0.6	0.1	179.1037, 161.0974, 135.1172, 133.0999	4	Loliolide II	Monoterpene lactone	Solanum lyratum	Solanaceae	9.51E+05	1.96
3	4.66	187.097 2		188.104 9	N	C ₉ H ₁₆ O ₄	98.5	2.0 8	0.3 9	125.0946	2	4,4- dimethylheptane dioic acid	Organic acids	Solanum melo ngena	Solanaceae	1.54E+05	0.32
4	6.72		371.1471	370.139 5	P	C ₂₁ H ₂₂ O ₆	76.5	5.6	2.1	N.D.	11	8-(2- hydroxypropan- 2-yl)-5- hydroxy-7- methoxy-6- methyl-4'- methoxyflavone	Flavones	Nioctiana tabacum	Solanaceae	9.34E+04	0.19
5	7.71		371.1472	370.139 5	P	C ₂₁ H ₂₂ O ₆	81.6	4.8	1.8	293.1015, 275.1259, 251.0910, 221.0578	11	8-(2- hydroxypropan- 2-yl)-5- hydroxy-7- methoxy-6- methyl-4'- methoxyflavone	Flavones	Nioctiana tabacum	Solanaceae	3.51E+05	0.72
6	8.46		235.1689	234.161	P	C ₁₅ H ₂₂ O ₂	90.2	1.9	0.4	N.D.	5	Lyciiterpenoid C/(28)-2-(2- hydroxypropan- 2-yl)-5,8- dimethyl- 1,2,3,4- tetrahydronapht halen-2-ol I	Eudesmane sesquiterpenes	Lycium chinense	Solanaceae	1.89E+05	0.39
7	8.58		371.1469	370.139 5	P	C ₂₁ H ₂₂ O ₆	83.8	5.9	2.2	N.D.	11	8-(2- hydroxypropan- 2-yl)-5- hydroxy-7- methoxy-6- methyl-4'- methoxyflavone III	Flavones	Nicotiana tab acum	Solanaceae	2.41E+05	0.50
8	11.9		199.1329	198.126 1	P	C ₁₁ H ₁₈ O ₃	90.7	2.3 1	-0.5	163.1041, 145.0964, 130.0739	3	(-)- Hydroxydihydro bovolide	α-β- unsaturatedγ- lactone	Solanum nigrum	Solanaceae	2.73E+05	0.56
9	13.3	691.357 2		692.363 5	N	C ₃₃ H ₅₆ O ₁₅	84	3.5 6	-2.5	397.1384, 293.2135, 275.2042, 235.0837	6	Pyishiauoside Ib I	Sesquiterpene saponins	Sapindus mukorossi	Sapindaceae	7.83E+04	0.16
10	13.5		217.1587	216.151 4	P	C ₁₅ H ₂₀ O	86.9	0.0 6	0.0 1	119.0856	6	(+)-anhydro-β- rotunol I	Vetispirane sesquiterpenes	Solanum lyratum	Solanaceae	3.22E+05	0.67
11	13.5	691.356		692.363 5	N	C ₃₃ H ₅₆ O ₁₅	83.7	2.2	-1.6	397.1368, 293.2118, 275.2023, 235.1711	6	Pyishiauoside Ib II	Sesquiterpene saponins	Sapindus mukorossi	Sapindaceae	7.74E+04	0.16
12	13.8		309.2066	308.198 9	P	C ₁₈ H ₂₈ O ₄	94.2	0.3 7	-0.1	291.2011, 273.2002, 245.1984, 231.1712	5	2- hydroxysolajian gxin E/ 7- hydroxylsolajian gxin I	Vetispirane sesquiterpenes	Solanum lyratum	Solanaceae	3.55E+05	0.73
13	15.1		257.1515	234.161	P	C ₁₅ H ₂₂ O ₂	97.1	2.7	0.6	N.D.	5	Lycilterpenoid C/(2S)-2-(2- hydroxypropan- 2-yl)-5,8- dimethyl- 1,2,3,4- tetrahydronapht halen-2-ol II	Eudesmane sesquiterpenes	Lycium chinense	Solanaceae	7.68E+05	1.58
14	15.4		257.1531 *	234.161	P	C ₁₅ H ₂₂ O ₂	82.9	1.9	-0.5	199.1482, 157.1013	5	Lyciiterpenoid C/(28)-2-(2- hydroxypropan- 2-yl)-5,8- dimethyl- 1,2,3,4- tetrahydronapht halen-2-ol III	Eudesmane sesquiterpenes	Lycium chinense	Solanaceae	2.04E+05	0.42
15	16	999.468 1		1000.47 4	N	C ₄₅ H ₇₆ O ₂₄	88.4	2.6 1	-2.6	N.D.	8	Mukurozioside Ib I	Sesquiterpene saponins	Sapindus mukorossi	Sapindaceae	1.92E+04	0.04
16	16.5	999.466 9		1000.47 4	N	C ₄₅ H ₇₆ O ₂₄	94.1	1.6 7	-1.7	721.2404, 559.1854, 383.1207, 179.0564	8	Mukurozioside Ib II	Sesquiterpene saponins	Sapindus mukorossi	Sapindaceae	2.13E+05	0.44
17	16.6	231.139 5	233.1537	232.146 7	N/ P	C ₁₅ H ₂₀ O ₂	97.1	1.4 9	-0.4	175.0755, 133.0656	6	Lyciiterpenoid A/B I	Eudesmane sesquiterpenes	Lycium chinense	Solanaceae	2.19E+05	0.45

18	16.8	999.467		1000.47 4	N	C ₄₅ H ₇₆ O ₂₄	94.7	1.1 9	-1.2	N.D.	8	Mukurozioside Ib III	Sesquiterpene saponins	Sapindus mukorossi	Sapindaceae	3.36E+04	0.07
19	17.9	1000.48		1002.49	N	C ₄₅ H ₇₈ O ₂₄	90.8	3.0	-3.1	739.2456,7 21.2412, 559.1910, 383.1095 179.0550	7	Mukurozioside Ia	Sesquiterpene saponins	Sapindus mukorossi	Sapindaceae	2.95E+04	0.06
20	18.1	231.139 4	233.153	232.146 7	N/ P	C ₁₅ H ₂₀ O ₂	81.2	-0.7	-0.2	N.D.	6	Lyciiterpenoid A/B II	Eudesmane sesquiterpenes	Lycium chinense	Solanaceae	2.41E+04	0.05
21	18.2		257.1504	234.161	P	C ₁₅ H ₂₂ O ₂	78.8	-0.2	-0.1	199.042	5	Lyciiterpenoid C/(2S)-2-(2- hydroxypropan- 2-yl)-5,8- dimethyl- 1,2,3,4- tetrahydronapht halen-2-ol IV	Eudesmane sesquiterpenes	Lycium chinense	Solanaceae	1.57E+05	0.32
22	18.7	999.466		1000.47 4	N	C ₄₅ H ₇₆ O ₂₄	80.2	0.0 7	-0.1	N.D.	8	Mukurozioside Ib IV	Sesquiterpene saponins	Sapindus mukorossi	Sapindaceae	1.64E+04	0.03
23	19.1	595.288 8		596.296 6	N	C ₃₄ H ₄₄ O ₉	80.2	0.0	-0.1	415.2774, 315.0489, 279.2340	13	Salannin I	Limonoids	Azadirachta indica	Meliaceae	6.54E+05	1.35
24	20.2		277.2150	276.207 9	P	C ₁₈ H ₂₈ O ₂	94.9	3.8	1.0	215.1667	5	Stearidonic acid I	Fatty acids	Vincetoxicum funebre	Apocyanace ae	6.55E+05	1.35
25	20.3	595.289 2		596.296 6	N	C ₃₄ H ₄₄ O ₉	81.2	2.7	1.6 2	415.2754, 315.0472, 279.2339	13	Salannin II	Limonoids	Azadirachta indica	Meliaceae	7.68E+05	1.58
26	20.3	293.213 0		294.221 1	N	C ₁₈ H ₃₀ O ₃	97.7	2.3	-0.7	275.2009, 231.2084	4	9-oxo- 10E,12(Z/E)- octadecadienoic acid I	Fatty acids	Capsicum ann uum	Solanaceae	2.77E+05	0.57
27	20.4 0		277.2152	276.207 9	P	C ₁₈ H ₂₈ O ₂	93.2	4.3 9	1.2	233.1025	5	Stearidonic acid II	Fatty acids	Vincetoxicum funebre	Apocyanace ae	2.21E+06	4.55
28	20.5 4	293.213 1		294.221 1	N	C ₁₈ H ₃₀ O ₃	97.3	-2.8	-0.8	275.2035, 231.2101	4	9-oxo- 10E,12(Z/E)- octadecadienoic acid II	Fatty acids	Capsicum ann uum	Solanaceae	8.76E+05	1.81
29	20.7		277.2162	276.207 9	P	C ₁₈ H ₂₈ O ₂	99.6	0.0 6	-0	233.0412	5	Stearidonic acid III	Fatty acids	Vincetoxicum funebre	Apocyanace ae	1.96E+06	4.04
30	20.8 5	293.213 2		294.221 1	N	C ₁₈ H ₃₀ O ₃	96.6	3.3	-1	275.2008, 231.2120	4	9-oxo- 10E,12(Z/E)- octadecadienoic acid III	Fatty acids	Capsicum ann uum	Solanaceae	9.47E+05	1.95
31	21.4 7	291.197		292.204 5	N	C ₁₈ H ₂₈ O ₃	90.3	2.3	-0.7	272.6369	5	Colnelenic acid	Fatty acids	Solanum tuberosum	Solanaceae	1.98E+05	0.41
32	22.0 9	295.229 0		296.236 4	N	C ₁₈ H ₃₂ O ₃	81.5	3.8	-1.1	277.2185	3	(S)-Coriolic acid I	Fatty acids	Deprea subtriflora	Solanaceae	1.02E+05	0.21
33	22.1		235.169	234.161	P	C ₁₅ H ₂₂ O ₂	96.8	1.0	0.2	N.D.	5	Lyciiterpenoid C/(2S)-2-(2- hydroxypropan- 2-y1)-5,8- dimethyl- 1,2,3,4- tetrahydronapht halen-2-ol V	Eudesmane sesquiterpenes	Lycium chinense	Solanaceae	2.58E+05	0.53
34	22.4 6	295.228 7		296.236 4	N	C ₁₈ H ₃₂ O ₃	97.2	2.2 7	-0.7	277.2171, 233.2277	3	(S)-Coriolic acid II	Fatty acids	Deprea subtriflora	Solanaceae	2.67E+06	5.51
35	23.2 7	295.228 5		296.236 4	N	C ₁₈ H ₃₂ O ₃	90.4	3.2	-1	277.2170, 233.2268	3	(S)-Coriolic acid III	Fatty acids	Deprea subtriflora	Solanaceae	1.88E+05	0.39
36	23.4		217.1589	216.151 4	P	C ₁₅ H ₂₀ O	97.3	0.4 7	-0.1	119.0849	6	(+)-anhydro-β- rotunol II	Vetispirane sesquiterpenes	Solanum lyratum	Solanaceae	5.39E+06	###
37	23.6		225.1479	224.141 1	P	C ₁₃ H ₂₀ O ₃	89.1	0.4 6	0.1	N.D.	4	Blumenol A	Cyclohexanone s	Lycium barbarum	Solanaceae	4.52E+05	0.93
38	23.5 8	293.213 1	295.2272	294.221 1	N	C ₁₈ H ₃₀ O ₃	94.3	3.0 9	-0.9	249.2262	4	9-oxo- 10E,12(Z/E)- octadecadienoic acid IV	Fatty acids	Capsicum ann uum	Solanaceae	2.13E+05	0.44
39	23.6		203.1061	202.099	P	C ₁₃ H ₁₄ O ₂	88	1.9	0.3	N.D.	7	2,2-Dimethyl- 6,8-dihydro-2H- furo[3,4- g]chromene	Isobenzofurans	Nioctiana tabacum	Solanaceae	2.40E+05	0.50
40	23.8	293.212 8		294.221 1	N	C ₁₈ H ₃₀ O ₃	88.1	-3	-0.9	249.2261	4	9-oxo- 10E,12(Z/E)- octadecadienoic acid V	Fatty acids	Capsicum ann uum	Solanaceae	5.33E+05	1.10
41	24.5 1	297.244 1		298.250 9	N	C ₁₈ H ₃₄ O ₃	84.6 6	1.7 2	0.0	279.2335, 261.2161	2	Ricinoleic acid I	Fatty acids	Solanum dulcamara	Solanaceae	5.28E+04	0.11
42	24.6	293.213 1	295.2270	294.221 1	N	C ₁₈ H ₃₀ O ₃	81.5	3.1	-0.9	249.2260	4	9-oxo- 10E,12(Z/E)- octadecadienoic acid VI	Fatty acids	Capsicum ann uum	Solanaceae	1.71E+05	0.35
43	24.7		301.1415	300.133 9	P	C ₁₈ H ₂₀ O ₄	86.5	6.9	2.0	N.D.	9	Doitungbipheny l A I	Phenols	Nioctiana tabacum	Solanaceae	8.34E+05	1.72

44	24.7		279.1591	278.151 8	P	C ₁₆ H ₂₂ O ₄	98.3	0.1	0.0	149.0229, 121.0278	6	Dibutyl phthalate I	Organic acids	0	Solanaceae	7.05E+05	1.45
45	24.7 5	297.244 1		298.250 9	N	C ₁₈ H ₃₄ O ₃	83.6	2.3	0.6	279.23	2	Ricinoleic acid	Fatty acids	Solanum dulcamara	Solanaceae	5.67E+04	0.12
46	25		301.1415	300.133 9	P	C ₁₈ H ₂₀ O ₄	86.7	6.8	2.0	283.2850, 233.1601	9	Doitungbipheny l A II	Phenols	Nioctiana tabacum	Solanaceae	1.82E+06	3.76
47	25.1		279.1592	278.151 8	Р	C ₁₆ H ₂₂ O ₄	99.2	0.4 2	-0.1	149.0232, 121.0281	6	Dibutyl phthalate II	Organic acids	Lycium barbar um	Solanaceae	1.66E+06	3.41
48	25.2 5	199.170 8		200.178	N	C ₁₂ H ₂₄ O ₂	98.8	1.9 5	-0.8	N.D.	1	Lauric acid	Fatty acids	Mandragora autumnalis	Solanaceae	2.72E+05	0.56
49	25.3 1	205.16		206.167	N	C ₁₄ H ₂₂ O	99.1	1.1 1	-0.2	N.D.	4	β-Methylionone	Monoterpenes	Solanum lycopersicum	Solanaceae	3.49E+05	0.72
50	26		219.1738	218.166 5	P	C ₁₅ H ₂₂ O	97.7	2.4	0.5 2	121.1009	5	Solavetivone I	Vetispirane sesquiterpenes	Solanum lyratum	Solanaceae	8.41E+05	1.74
51	27.5		219.1748	218.166 5	P	C ₁₅ H ₂₂ O	98.1	1.8 2	-0.4	N.D.	5	Solavetivone II	Vetispirane sesquiterpenes	Solanum lyratum	Solanaceae	2.35E+05	0.49
52	29.3 8	277.218 5		278.225 2	N	C ₁₈ H ₃₀ O ₂	95.1	3.8	-1.1	259.2063, 233.1761	4	Linolenic acid	Fatty acids	Withania somnifera	Solanaceae	2.96E+06	6.12
53	29.8 8	227.202 1		228.209 4	N	C ₁₄ H ₂₈ O ₂	99	2.1 1	-0.5	209.189	1	Myristic acid	Fatty acids	Hyoscyamus niger	Solanaceae	5.50E+05	1.14
54	30.1 2		256.2633	255.256 0	P	C ₁₆ H ₃₃ N O	99	1.1 2	0.6 8	238.2503, 186.1813	1	Palmitamide	Long-chain amides	Boronia koniambiensis	Rutaceae	1.48E+06	3.06
55	31.0 5		270.2787	269.269 2	P	C ₁₇ H ₃₅ N O	83.8	3.7 4	1.0 1	N.D.	1	N- methylpalmitam ide	Long-chain amides	Gossypium hirsutum	Malvaceae	2.90E+04	0.06
56	31.4 2	279.234 1	281.2475	280.241 3	N/ P	C ₁₈ H ₃₂ O ₂	95.1	3.8	-1.1	261.2214	3	Linoleic acid I	Fatty acids	Nioctiana tabacum	Solanaceae	4.04E+06	8.34
57	31.8 5	279.233 5		280.241 3	N	C ₁₈ H ₃₂ O ₂	95.9	1.5 5	-0.4	261.2919	3	Linoleic acid II	Fatty acids	Nioctiana tabacum	Solanaceae	3.38E+05	0.70
58	33.2 1	255.234 5		256.241 6	N	C ₁₆ H ₃₂ O ₂	91.3	5.4 7	-1.4	237.2208, 223.0634	1	Palmitic acid	Fatty acids	Solanum chac oense	Solanaceae	4.14E+06	8.55
59	33.5 2	281.249 5		282.255 9	N	C ₁₈ H ₃₄ O ₂	95.6	3.4	-1	263.0233	2	Oleic acid I	Fatty acids	Nioctiana tabacum	Solanaceae	1.48E+06	3.06
60	33.9 6	281.248 6		282.255 9	N	C ₁₈ H ₃₄ O ₂	88.8	0.6 2	-0.2	N.D.	2	Oleic acid II	Fatty acids	Nioctiana tabacum	Solanaceae	1.36E+05	0.28
61	35.5 7	283.265 7		284.272 4	N	C ₁₈ H ₃₆ O ₂	71.8	4.1	-1.1	N.D.	1	Stearic acid I	Fatty acids	Solanum chaco ense	Solanaceae	2.39E+04	0.05
62	35.8 8	283.265 0		284.272 4	N	C ₁₈ H ₃₆ O ₂	96.1	2.0 5	-0.6	265.2511	1	Stearic acid II	Fatty acids	Solanum chaco ense	Solanaceae	3.22E+05	0.66
		ium adduct, vest value	N; negative, P	; positive, N.		letected, DBE thest value.	, Double	bond e	quivalen	ce							

Table 2 : Molecular docking analysis of the extracted compounds against GSK3- β , HIF Hydroxylase, KEAP1-Nrf2 complex and PTEN.

Tested compounds	Compounds	RMSD value (Å)	Docking (Affinity) score (kcal/mol)
GSK3-β	2-hydroxysolajiangxin-E	0.98	-6.98
	Salannin I-II	1.06	-9.45
	Doitungbiphenyl-A I-II	1.35	-7.02
	Co-crystalized ligand	0.83	-7.11
	(Morin)		
HIF	2-hydroxysolajiangxin-E	0.81	-6.77
Hydroxylase	Blumenol A	0.85	-6.62
	Co-crystalized ligand	0.65	-5.90
	(R8J)		
KEAP1-Nrf2	2-hydroxysolajiangxin-E	1.10	-6.86
complex	Blumenol-A	1.62	-7.12
	Co-crystalized ligand	1.03	-6.97
	(J6H)		
PTEN	Lyciiterpenoid-C I-V	1.74	-5.99
	Lyciiterpenoid-A	1.47	-5.85
	Co-crystalized ligand	1.21	-4.12
	(SJA)		

functional group, the phenyl group and the methoxy contribute to the high binding.

However, the lower binding affinity of 2-hydroxysolajiangxin-E compared to salannin I-II indicates that the absence of the ester groups and different substituents on the hydroxyl groups on 2-hydroxysolajiangxin-E leads to the difference observed and contributes to weaker interactions with GSK3- β (Fig. 10). For HIF Hydroxylase, a key regulator of angiogenesis through its control of HIF-1 α stability [76,77], 2-hydroxysolajiangxin-E displayed a docking score of -6.77 kcal/mol. This interaction was characterized by eleven hydrophobic π -Alkyl interactions with Trp389, Met299, Tyr310, Val376, Ile327, His374, and His313 and two hydrogen bonds with Arg322, and Tyr303 with bond length of 2.29, and 1.97 Å (Fig. 11).

Similarly, blumenol-A exhibited a comparable binding affinity of -6.62 kcal/mol for HIF Hydroxylase (Fig. 12), compared with the cocrystalized ligand (R8J) which exhibited an affinity score of -5.90 kcal/mol and formed three hydrophobic π -interactions with Val376, and Trp389, and furthermore interacted with His313, and Tyr303 by two hydrogen bonds with distances of 3.30, and 1.79 Å, respectively (Fig. 13).

blumenol-A formed eleven hydrophobic π -sigma, and π -Alkyl interactions with His374, Val376, Ala385, Tyr303, His313, Ile327, Tyr329, Leu343, and Tyr310 and moreover, it interacted with Tyr303,

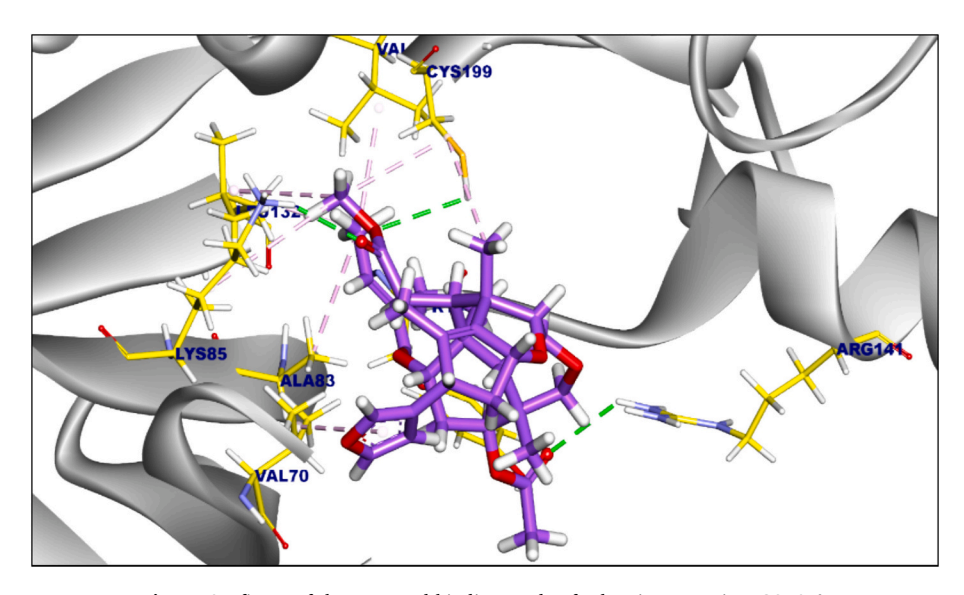


Fig. 7. 3D figure of the proposed binding mode of salannin I-II against GSK3-β.

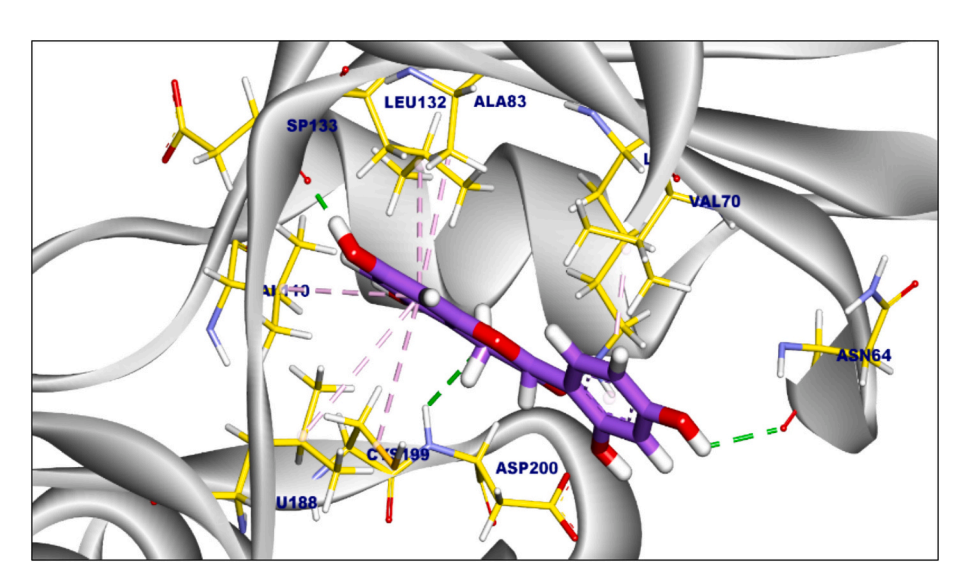


Fig. 8. 3D figure of the proposed binding mode of the co-crystalized ligand (Morin) complexed with GSK3-β.

and Arg383 by two hydrogen bonds with distances of 1.79, and 2.21 Å (Fig. 12). The comparable binding affinity and common hydrophobic interactions and one hydrogen bond interaction between 2-hydroxysolajiangxin-E and blumenol-A with the active site of HIF Hydroxylase suggest that the presence of the hydroxyl group, the ketone group, and the methyl substituent on the five-membered ring in both 2-hydroxysolajiangxin-E and blumenol-A are the most important contributors. This contrasts with the key elements in Salannin I-II that have good binding for GSK3-β, suggesting the presence of a hydroxyl group or lactone ring is a better interaction in the active site over a decalin substituent. The KEAP1-Nrf2 complex was another target of interest, as this complex has a demonstrated role in promoting wound healing [76–78]. blumenol-A) showed the highest binding affinity (-7.12 kcal/mol) for this complex, facilitated by four hydrophobic π -Alkyl interactions with Phe577, Tyr572, Tyr525, and Ala556 and four hydrogen bonds with Ser602, Ser555, Arg483, and Ser508 with distances of 2.19, 2.39, 2.22, and 2.77 Å (Fig. 14), compared to an affinity of -6.97 kcal/mol for the cocrystalized ligand (J6H) which formed five hydrophobic π - π , π -cation, π -anion, and π -Alkyl interactions with Tyr525, Phe478, Arg415, and Ala556, and further interacted with Ser508, Arg483, Ser555, and Gln530 by four hydrogen bonds with distances of 1.84, 1.86, 1.71, and

1.90 Å, respectively (Fig. 10 and. Fig. 15).

2-hydroxysolajiangxin-Ealso showed a comparable affinity of -6.86 kcal/mol as it formed four hydrophobic π -alkyl interactions with Ala556, Tyr334, Phe577, and Tyr572 and, additionally, by three hydrogen bonds the interaction was established with Arg483, Ser508, and Arg415 with distances of 2.19, 2.82, and 2.49 Å, (Fig. 16).

The close binding affinity between compounds, 2-hydroxysolajiang-xin-E and blumenol-A may be attributed to their respective structural features and polar functional groups capable of hydrogen bonding and is also shown by the position of methyl substituents on the cyclic compounds. A comparison with Salannin I-II, which showed a poor KEAP1-Nrf2 binding affinity, suggests the absence of both a 5-membered ring with hydroxyl and the hydroxyl substituent, and the absence of a position for these functional groups, such as the decalin ring system that does not allow it, leads to poorer docking results, where the spatial structure and substituents play an important role.

PTEN, a phosphatase that regulates cell proliferation, survival, and migration, all of which are important for wound closure, was also examined [79,80]. Lycitterpenoid C I-V demonstrated the most favorable binding affinity for PTEN, with a docking score of -5.99 kcal/mol (Fig. 17).

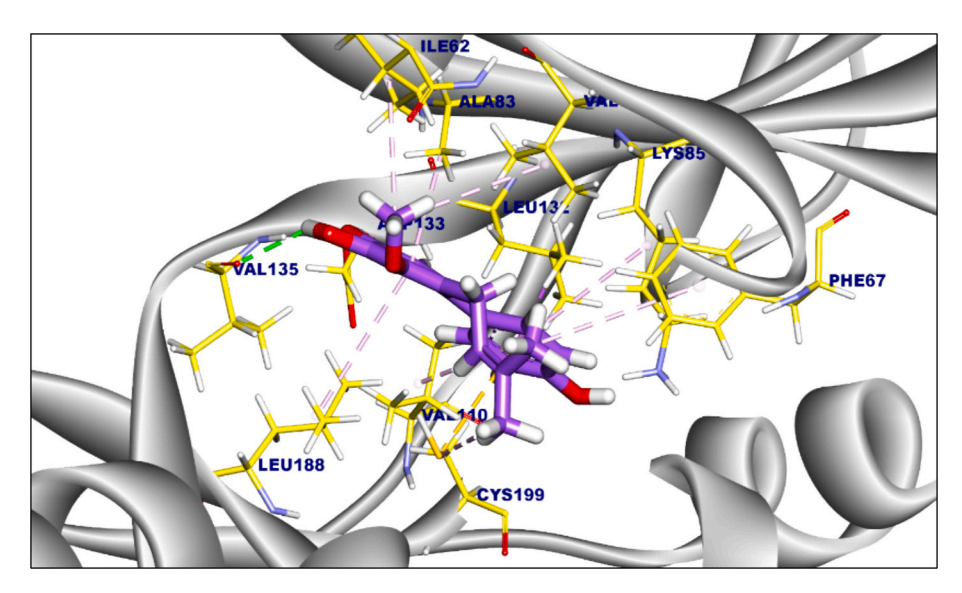


Fig. 9. 3D figure of the proposed binding mode of doitungbiphenyl A I-II against GSK3- β .2-hydroxysolajiangxin E also exhibited a notable binding affinity for GSK3- β (-6.98 kcal/mol), forming seven hydrophobic π -alkyl interactions with Cys199, Leu188, Val70, and Tyr134 and two hydrogen bonds with Lys85, and Arg141 with distances of 2.29, and 2.50 Å (Fig. 10).

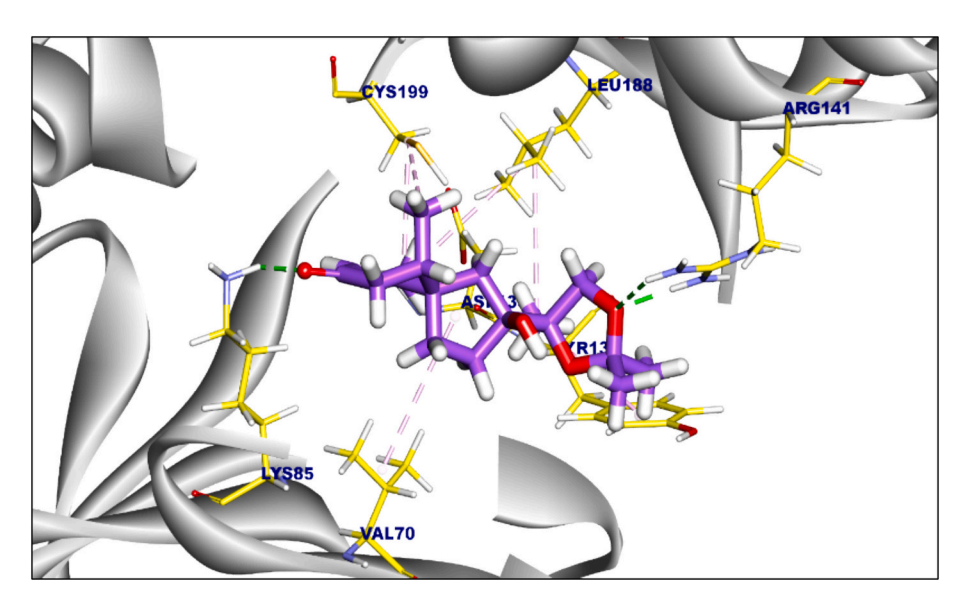


Fig. 10. 3D figure of the proposed binding mode of 2-hydroxysolajiangxin-E against GSK3-β.

This interaction was mediated by eight hydrophobic $\pi\text{-}\pi$ and $\pi\text{-}Alkyl$ interactions with Phe280, Leu192, Phe196, Ala189, and Val287. On the other hand, it interacted with Asn193 by a hydrogen bond with a distance of 2.06 Å (Fig. 17). The Co-crystalized ligand SJA displayed a binding affinity of -4.12 kcal/mol (Fig. 18).

This suggests that the tetrahydronaphthalene ring system and its hydrophobic faces, and the propanol group for the creation of the hydrogen bond, are essential characteristics in the active site. Lyciiterpenoid-A exhibited an affinity score of -5.85 kcal/ mol. it was formed nine hydrophobic π -Alkyl interactions with Leu192, Phe280, Phe196, Ala189, and Val287. Additionally, two hydrogen bonds were observed with Glu276, and Ala189 with distances of 1.84 (Fig. 19).

The slightly improved binding affinity compared to lyciiterpenoid-C I-V to the active site, highlights the significance of the

tetrahydronaphthalene ring system and the hydroxyl for the formation of hydrogen bonds.

Collectively, the *in-silico* docking studies revealed that the six examined L. shawii metabolites exhibited varying degrees of affinity for key regulatory proteins involved in angiogenesis and wound repair. These binding differences point to potential structure-activity relationships. The docking scores of the co-crystalized ligands confirm the validity of our method. Furthermore, our in vivo data demonstrating increased VEGF expression provides additional support for the potential role of these compounds in promoting angiogenesis. While Salannin I-II displayed the strongest affinity for GSK3- β , 2-hydroxysolajiangxin-E and blumenol A showed promising interactions with HIF Hydroxylase and the KEAP1-Nrf2 complex. Lyciiterpenoid-C I-V showed the most favorable binding for PTEN. These findings suggest that different structural

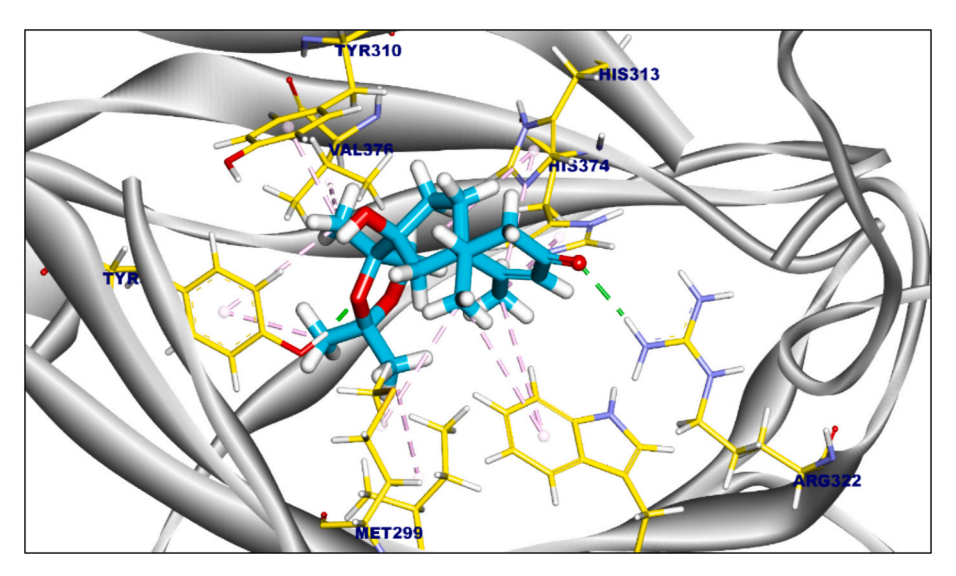


Fig. 11. 3D figure of the proposed binding mode of 2-hydroxysolajiangxin-E against HIF Hydroxylase.

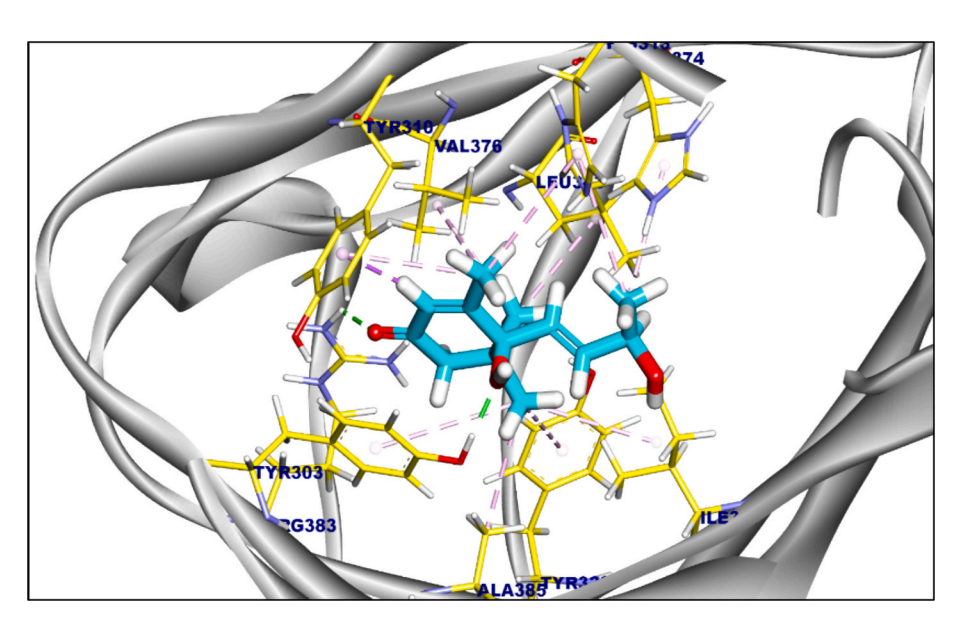


Fig. 12. Figure of the proposed binding mode of blumenol A against HIF Hydroxylase.

features may be important for targeting each protein. These findings suggest that *L. shawii* extracts may promote wound healing through multiple mechanisms, primarily through enhanced VEGF and increased angiogenesis.

3.4. Pharmacokinetics, toxicity and drug likeness (ADME/Tox), in-silico prediction

The in silico ADMET (Absorption, Distribution, Metabolism, Excretion, and Toxicity) profiles of the six tested compounds (with excellent binding affinities to the targets) derived from *L. shawii* extract were predicted using the Deep-PK online tool, and the results are compiled in (Table 3).

This analysis provides an initial assessment of the compounds' potential as drug candidates, emphasizing key parameters relevant to bioavailability, distribution, metabolic fate, and potential toxicity.

Key physicochemical properties revealed the logarithm of the n-octanol/water distribution coefficient (log D7.4), as a measure of lip-ophilicity at physiological pH (7.4), ranging from 0.5 to 4.48. Log *P* values ranged between 0.47 and 5.73, suggesting an overall appropriate

range for crossing cellular membranes. Furthermore, the negative S values, (from -1 to -6), indicate low water solubility and potential stability.

The Human Oral Bioavailability (HOB) predictions demonstrated favorable values across all compounds. Lyciiterpenoid-C I-V, (0.792), Lyciiterpenoid-A (0.763), blumenol-A (0.789), Salannin I-II (0.762), Doitungbiphenyl-A I-II (0.699), and 2-hydroxysolajiangxin-E (0.839) all exhibited values above 0.699, signifying a high probability of oral absorption. Supporting this, permeability across the intestinal epithelium, simulated by Caco-2 cell permeability values, indicated permeability through the cell membrane, ranging from $-4.55\ \text{to}\ -5.01.$

In terms of distribution, Blood-Brain Barrier (BBB) permeability predictions suggest variability, with compounds, Lyciiterpenoid-C I-V, Lyciiterpenoid-A, and blumenol-A predicted to cross the BBB.

The compounds also exhibited high protein-binding ability, as exemplified by Lyciiterpenoid-A (60.47) and Doitungbiphenyl-A I-II (66.71), which is consistent to a low $SSVDf_f$ (stead state distribution) indicating less body distribution. The CYP (Cytochrome P450) metabolism predictions revealed all compounds as substrates for these enzymes. For our investigation, Salannin I-II and Doitungbiphenyl-A I-II

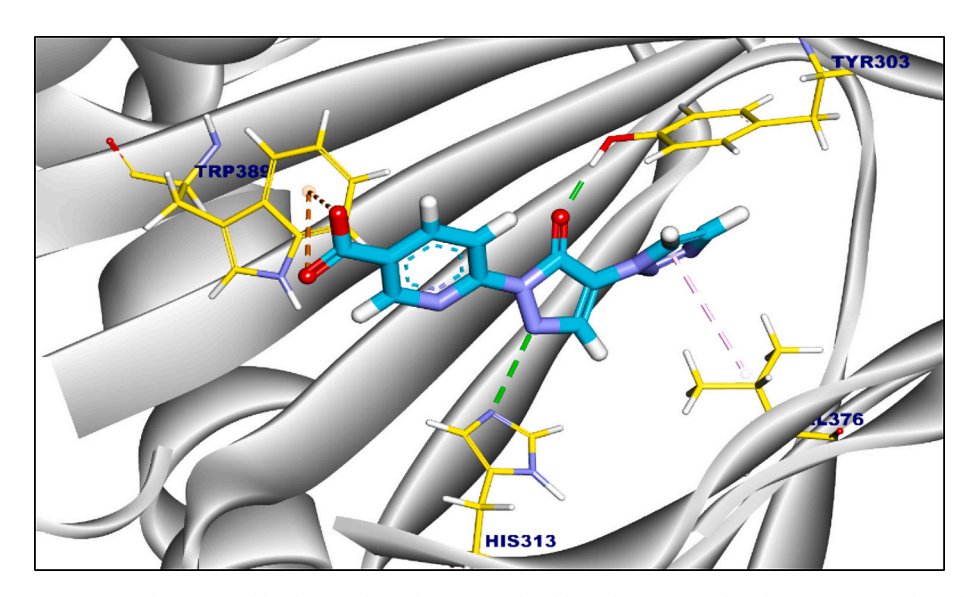


Fig. 13. Figure of the proposed binding mode of the co-crystalized ligand (R8J) complexed against HIF Hydroxylase.

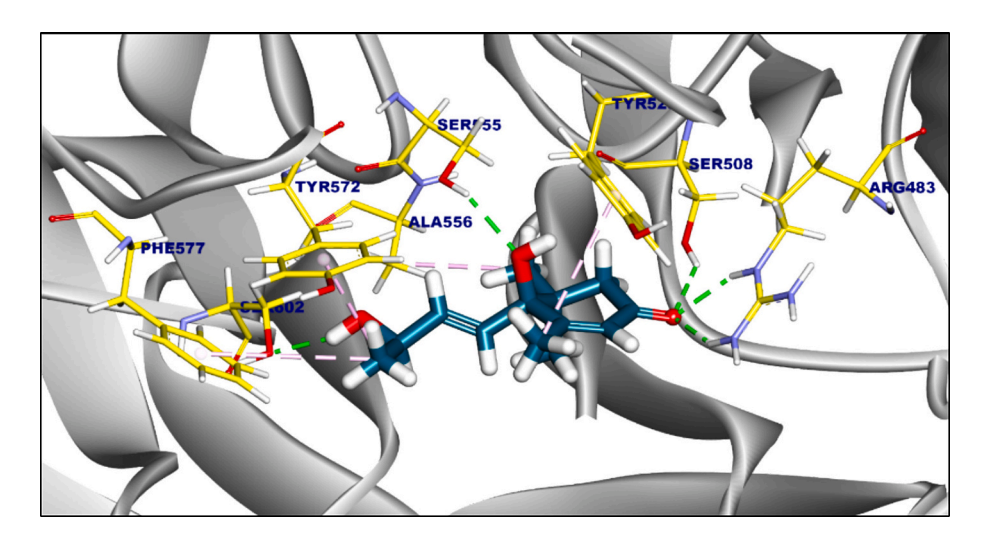


Fig. 14. 3D figure of the proposed binding mode of Blumenol-A against KEAP1-Nrf2 complex.

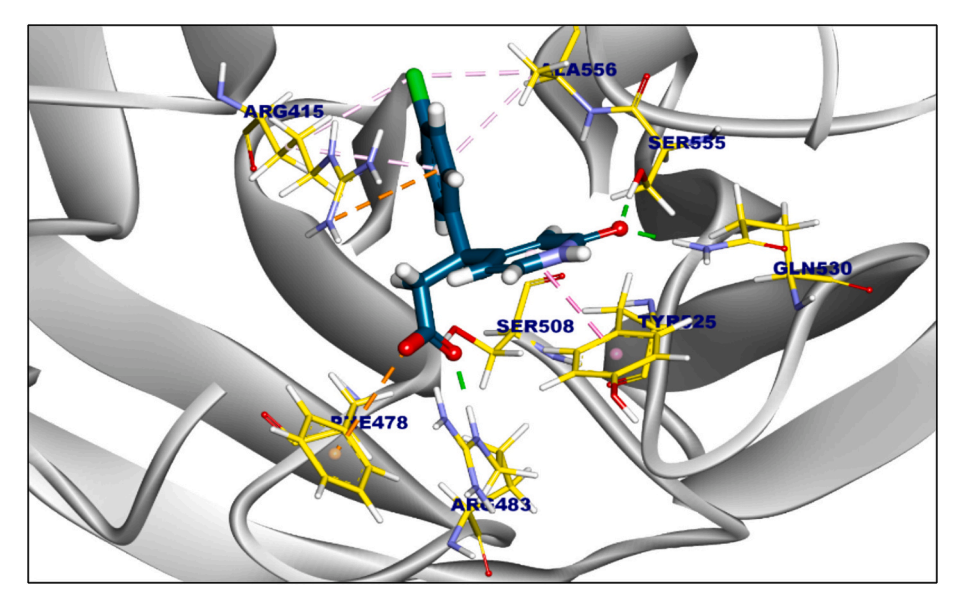


Fig. 15. 3D figure of the proposed binding mode of the co-crystalized ligand (J6H) against KEAP1-Nrf2 complex.

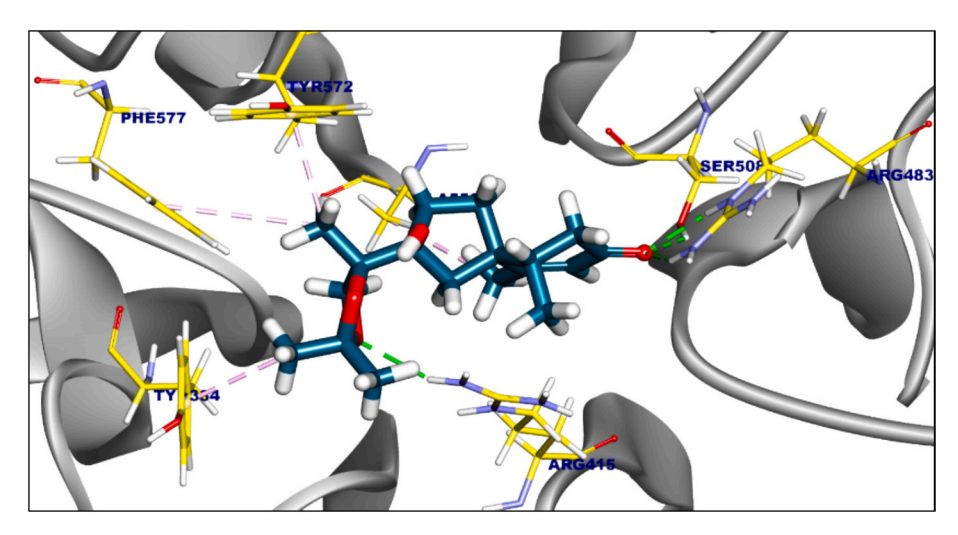


Fig. 16. Figure of the proposed binding mode of 2-hydroxysolajiangxin-E against KEAP1-Nrf2 complex.

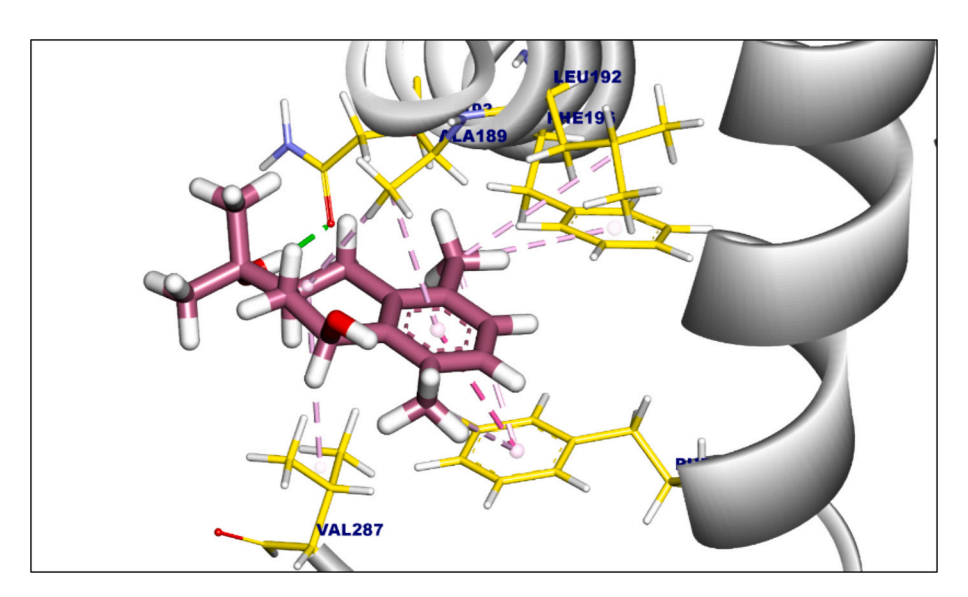


Fig. 17. 3D figure of the proposed binding mode of Lyciiterpenoid-C I-V against PTEN.

showed a good inhibition capacity against the P450 isoform. Finally, the toxicity evaluation revealed generally low and safe profiles; however, some members were considered toxic or unsafe based on predictions. Additionally, it is crucial to note that these *in-silico* predictions, while valuable for initial screening, are not definitive and require experimental validation. The toxicity flags identified, such as for AMES mutagenesis, serve as preliminary warnings that necessitate rigorous safety evaluation before any clinical consideration. Future work must therefore prioritize experimental confirmation through in vitro assays for cytotoxicity and mutagenicity, and subsequent in vivo dermal sensitization studies to definitively establish a safe profile for topical application. This validation is a critical step to bridge our computational findings with translational potential. Having established the significant in vivo efficacy of the L. shawii extract, the translational pathway to a clinical product necessitates a rigorous pharmaceutical development phase. This subsequent stage must address the comprehensive characterization of the delivery vehicle, a scope intentionally deferred in the present study. Future investigations are therefore imperative to define crucial formulation parameters, including long-term physicochemical stability, drug release kinetics, and skin permeation profiles. Establishing a robust, reliable, and effective formulation through such studies is essential to translate the potent biological activity demonstrated herein

into a viable therapeutic.

Indeed, this comprehensive investigation was strategically executed using a modern chemo-centric approach, where the comprehensive metabolomic characterization of the extract served as the foundation for all subsequent inquiries. Molecular docking, followed by in-silico ADME/ toxicity analysis, was then leveraged as a powerful chemo-informatic screening tool to rationally prioritize metabolites with high predicted affinity for key wound-healing targets. The subsequent in vivo evaluation of the crude extract was therefore not merely exploratory but served as the pivotal experimental validation of our central hypothesis: that the synergistic action of these computationally identified lead compounds would manifest as significant, measurable biological efficacy. While definitive mechanistic conclusions for individual compounds are intentionally deferred to subsequent bioassay-guided isolation studies, the present work successfully bridges the gap from chemical composition to validated therapeutic potential, providing a robust foundation for the targeted development of its most promising constituents.

4. Conclusion

This study comprehensively evaluated the wound-healing potential of *L. shawii* methanolic extract using a multi-modal approach. In vivo

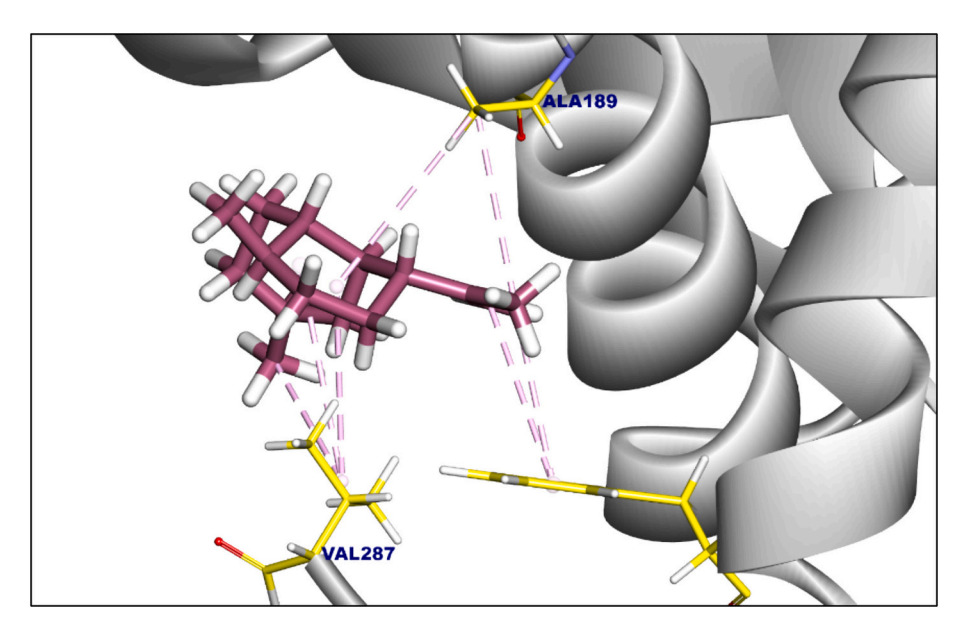


Fig. 18. 3D figure of the proposed binding mode of the co-crystallized ligand (SJA) against PTEN.

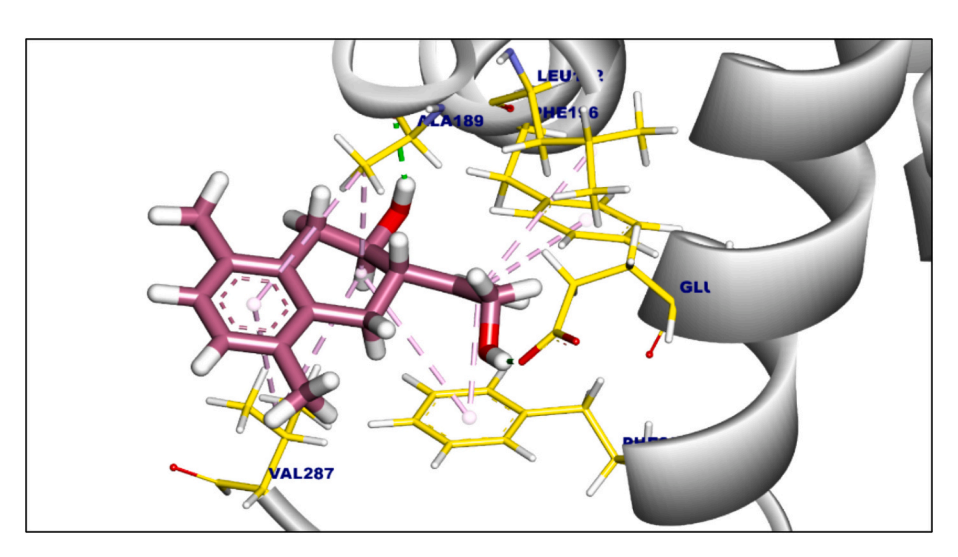


Fig. 19. 3D figure of the proposed binding mode of Lyciiterpenoid A against PTEN.

experiments demonstrated significant wound contraction (88.63 % by day 14) and enhanced collagen deposition, effectively paralleling the performance of the standard Fucidin®. Histopathological and immunohistochemical analyses further revealed reduced inflammation, accelerated re-epithelization, and upregulated VEGF expression, underscoring the extract's pro-angiogenic activity. Metabolic profiling identified 62 secondary metabolites, including terpenes, fatty acids, and phenolic compounds, suggesting a synergistic mechanism of action. In silico molecular docking corroborated these findings, demonstrating strong interactions between key metabolites (e.g., salannin I-II, 2hydroxysolajiangxin-E) and crucial wound-healing targets such as GSK3-β, HIF Hydroxylase, and KEAP1-Nrf2, thus supporting the observed VEGF upregulation and modulation of oxidative stress and angiogenesis pathways. Favorable ADMET predictions indicated acceptable oral bioavailability and low toxicity risks for the active compounds, strengthening their pharmaceutical potential. Although Fucidin® exhibited superior performance in some respects, L. shawii presents a compelling natural, multi-targeted therapeutic alternative with a potentially reduced risk of adverse effects. Future research should prioritize the isolation of individual bioactive compounds, optimization

of clinical formulations, and validation through human clinical trials. This work highlights the significance of integrating traditional herbal medicine knowledge with contemporary computational and experimental methodologies to facilitate the development of safe and effective wound-healing therapies.

CRediT authorship contribution statement

Mahmoud Moustafa: Writing – review & editing, Writing – original draft, Visualization, Formal analysis, Data curation, Conceptualization. Walaa S. Aboelmaaty: Writing – review & editing, Writing – original draft, Formal analysis, Data curation, Conceptualization. Weaam Ebrahim: Writing – review & editing, Writing – original draft, Formal analysis, Data curation, Conceptualization. Reham Hassan Mekky: Writing – review & editing, Writing – original draft, Visualization, Validation, Formal analysis, Data curation. Mohamed A. Tammam: Writing – review & editing, Writing – original draft, Amr El-Demerdash: Writing – review & editing, Writing – original draft, Visualization, Validation, Supervision, Software, Resources, Project administration, Methodology, Investigation, Funding acquisition, Formal analysis, Data

Table 3
ADME/Tox profiling of six selected compounds.*

Human Intestinal Absorption Skin Permeability Distribution Blood-Brain Barrier Plasma Protein Binding SSVDff Metabolism CYP 1A2, CYP 2C19, CYP 2D6, OATP1B1 Inhibitor CYP 1A2, CYP 2C19, CYP 2D6 Substrate CYP 2C9, CYP 3A4 Inhibitor CYP 2C9, CYP 3A4 Substrate Not	2.2 2.84 -2.45 -4.61 oavailable (0.792) rbed (0.994) -2.85	1.86 2.65 -2.47 -4.68 Bioavailable (0.763) Absorbed (0.995)	4.48 5.73 -6.15 -5.01 Bioavailable	2.53 3.9 -4.29	0.5 0.47 -0.95	1.91 2.68 -2.72
log P log S Absorption Caco-2 permeability Human Oral Bioavailability 20 % Human Intestinal Absorption Skin Permeability Distribution Blood-Brain Barrier Plasma Protein Binding SSVDff Metabolism CYP 1A2, CYP 2C19, CYP 2D6, OATP1B1 Inhibitor CYP 1A2, CYP 2C19, CYP 2D6 Substrate CYP 2C9, CYP 3A4 Inhibitor No CYP 2C9, CYP 3A4 Substrate	2.84 -2.45 -4.61 oavailable (0.792) rbed (0.994)	2.65 -2.47 -4.68 Bioavailable (0.763) Absorbed (0.995)	5.73 -6.15 -5.01 Bioavailable	3.9 -4.29	0.47 -0.95	2.68 -2.72
log S Absorption Caco-2 permeability Human Oral Bioavailability 20 % Bio Human Intestinal Absorption Skin Permeability Distribution Blood-Brain Barrier Penet Plasma Protein Binding SSVDff Metabolism CYP 1A2, CYP 2C19, CYP 2D6, OATP1B1 Inhibitor CYP 1A2, CYP 2C19, CYP 2D6 Substrate CYP 2C9, CYP 3A4 Inhibitor No CYP 2C9, CYP 3A4 Substrate	-2.45 -4.61 oavailable (0.792) rbed (0.994)	-2.47 -4.68 Bioavailable (0.763) Absorbed (0.995)	−6.15 −5.01 Bioavailable	-4.29 -4.85	-0.95	-2.72
Absorption Caco-2 permeability Human Oral Bioavailability 20 % Bio Human Intestinal Absorption Skin Permeability Distribution Blood-Brain Barrier Plasma Protein Binding SSVDff Metabolism CYP 1A2, CYP 2C19, CYP 2D6, OATP1B1 Inhibitor CYP 1A2, CYP 2C19, CYP 2D6 Substrate CYP 2C9, CYP 3A4 Inhibitor No	-4.61 oavailable (0.792) rbed (0.994)	-4.68 Bioavailable (0.763) Absorbed (0.995)	–5.01 Bioavailable	-4.85		
Caco-2 permeability Human Oral Bioavailability 20 % Bio Human Intestinal Absorption Skin Permeability Distribution Blood-Brain Barrier Penet Plasma Protein Binding SSVDff Metabolism CYP 1A2, CYP 2C19, CYP 2D6, OATP1B1 Inhibitor CYP 1A2, CYP 2C19, CYP 2D6 Substrate CYP 2C9, CYP 3A4 Inhibitor No CYP 2C9, CYP 3A4 Substrate	oavailable (0.792) rbed (0.994)	Bioavailable (0.763) Absorbed (0.995)	Bioavailable		_4.68	
Human Oral Bioavailability 20 % Bio Human Intestinal Absorption Skin Permeability Distribution Blood-Brain Barrier Plasma Protein Binding SSVDff Metabolism CYP 1A2, CYP 2C19, CYP 2D6, OATP1B1 Inhibitor CYP 1A2, CYP 2C19, CYP 2D6 Substrate CYP 2C9, CYP 3A4 Inhibitor No CYP 2C9, CYP 3A4 Substrate	oavailable (0.792) rbed (0.994)	Bioavailable (0.763) Absorbed (0.995)	Bioavailable		_4 68	
Human Intestinal Absorption Skin Permeability Distribution Blood-Brain Barrier Plasma Protein Binding SSVDff Metabolism CYP 1A2, CYP 2C19, CYP 2D6, OATP1B1 Inhibitor CYP 1A2, CYP 2C19, CYP 2D6 Substrate CYP 2C9, CYP 3A4 Inhibitor No. CYP 2C9, CYP 3A4 Substrate No.	(0.792) orbed (0.994)	(0.763) Absorbed (0.995)			-4.00	-4.55
Skin Permeability Distribution Blood-Brain Barrier Plasma Protein Binding SSVDff Metabolism CYP 1A2, CYP 2C19, CYP 2D6, OATP1B1 Inhibitor CYP 1A2, CYP 2C19, CYP 2D6 Substrate CYP 2C9, CYP 3A4 Inhibitor CYP 2C9, CYP 3A4 Substrate Not			(0.762)	Bioavailable (0.699)	Bioavailable (0.789)	Bioavailable (0.839)
Blood-Brain Barrier Penet Plasma Protein Binding SSVDff Metabolism CYP 1A2, CYP 2C19, CYP 2D6, OATP1B1 Inhibitor CYP 1A2, CYP 2C19, CYP 2D6 Substrate CYP 2C9, CYP 3A4 Inhibitor CYP 2C9, CYP 3A4 Substrate Not		-2.98	Absorbed (0.927) 10.39	Absorbed (0.954) -1.63	Absorbed (0.977) -2.66	Absorbed (0.992) -2.43
Plasma Protein Binding SSVDff Metabolism CYP 1A2, CYP 2C19, CYP 2D6, OATP1B1 Inhibitor CYP 1A2, CYP 2C19, CYP 2D6 Substrate CYP 2C9, CYP 3A4 Inhibitor CYP 2C9, CYP 3A4 Substrate Not						
SSVDff Metabolism CYP 1A2, CYP 2C19, CYP 2D6, No. OATP1B1 Inhibitor CYP 1A2, CYP 2C19, CYP 2D6 Substrate CYP 2C9, CYP 3A4 Inhibitor No. CYP 2C9, CYP 3A4 Substrate	rable (0.991)	Penetrable (0.938)	Penetrable (0.969)	Non-Penetrable (0.005)	Penetrable (1)	Penetrable (0.999)
Metabolism CYP 1A2, CYP 2C19, CYP 2D6, No. OATP1B1 Inhibitor CYP 1A2, CYP 2C19, CYP 2D6 Substrate CYP 2C9, CYP 3A4 Inhibitor CYP 2C9, CYP 3A4 Substrate	17.56	60.47	20.78	66.71	17.84	46.68
CYP 1A2, CYP 2C19, CYP 2D6, OATP1B1 Inhibitor CYP 1A2, CYP 2C19, CYP 2D6 Substrate CYP 2C9, CYP 3A4 Inhibitor NO CYP 2C9, CYP 3A4 Substrate	1.8	2.33	2.82	1.16	0.99	1.14
OATP1B1 Inhibitor CYP 1A2, CYP 2C19, CYP 2D6 Substrate CYP 2C9, CYP 3A4 Inhibitor NO CYP 2C9, CYP 3A4 Substrate Noi						
Substrate CYP 2C9, CYP 3A4 Inhibitor CYP 2C9, CYP 3A4 Substrate Not	n-Inhibitor (0.021)	Non-Inhibitor (0.024)	Inhibitor (0.634)	Inhibitor (0.976)	Non-Inhibitor (0.01)	Non-Inhibitor (0.001)
CYP 2C9, CYP 3A4 Substrate Nor	trate (0.656)	Substrate (0.564)	Substrate (0.65)	Non-Substrate (0.373)	Non-Substrate (0.494)	Substrate (0.609)
CYP 2C9, CYP 3A4 Substrate Nor	n-Inhibitor (0.003)	Non-Inhibitor (0.003)	Inhibitor (0.753)	Non-Inhibitor (0.219)	Non-Inhibitor (0)	Non-Inhibitor (0.002)
	n-Substrate (0.294)	Non-Substrate (0.144)	Non-Substrate (0.383)	Non-Substrate (0.009)	Non-Substrate (0.005)	Non-Substrate (0.001)
Excretion						
Clearance	8.48	9.32	10.6	7.89	4.54	11.24
	n-Inhibitor (0.126)	Non-Inhibitor (0.096)	Non-Inhibitor (0.063)	Inhibitor (0.754)	Non-Inhibitor (0.072)	Non-Inhibitor (0.474)
Toxicity						
e	xic (0.851)	Safe (0.433)	Safe (0.003)	Safe (0.013)	Safe (0.306)	Toxic (0.563)
	fe (0.173)	Safe (0.071)	Safe (0.025)	Safe (0.037)	Safe (0.156)	Safe (0.079)
	xic (0.804)	Toxic (0.686)	Toxic (0.981)	Safe (0.469)	Toxic (0.78)	Toxic (0.988)
ĕ	afe (0.02)	Safe (0.036)	Safe (0.009)	Safe (0.006)	Safe (0.347)	Safe (0.119)
ē .	xic (0.628)	Safe (0.482)	Toxic (0.527)	Toxic (0.669)	Toxic (0.838)	Toxic (0.56)
	afe (0.28)	Safe (0.305)	Toxic (0.704)	Safe (0.073)	Safe (0.245)	Safe (0.056)
3 3	fe (0.236)	Safe (0.261)	Safe (0.438)	Toxic (0.669)	Safe (0.153)	Safe (0.208)
•	fe (0.001)	Safe (0.171)	Safe (0)	Safe (0.486)	Safe (0.008)	Safe (0)
•	afe (0.33)	Safe (0.171)	Safe (0.02)	Safe (0.484)	Toxic (0.556)	Safe (0.079)
Maximum Tolerated Dose	0.95	0.64	-0.35	0.78	0.86	0.04
3 3	xic (0.595)	Toxic (0.552)	Toxic (0.518)	Toxic (0.59)	Safe (0.483)	Toxic (0.581)
	Safe (0) xic (0.642)	Safe (0.005) Toxic (0.609)	Safe (0) Safe (0.242)	Safe (0.256) Toxic (0.518)	Safe (0) Toxic (0.597)	Safe (0) Toxic (0.638)

^{*} Probabilities and confidence levels are indicated in parentheses where applicable.

curation, Conceptualization. Ahmed M. Zaghloul: Writing – review & editing, Writing – original draft, Formal analysis, Data curation, Conceptualization.

Ethics approval

All animal handling and tissue preparation procedures were conducted in compliance with established ethical guidelines, with approval obtained from the Mansoura University Animal Care Committee (MU-ACUC) (Ethical Approval Code: 34–2025 (Approved on 26/03/2025).

Funding

This research did not receive any specific grant from funding agencies in the public, commercial, or not-for-profit sectors.

Declaration of competing interest

The authors declare that they have no known competing commercial interests or personal relationships that could have appeared to influence the work reported in this paper.

All authors have read and agreed to the published version of the manuscript.

Acknowledgments

Mohamed A. Tammam is humbly dedicating this work to the soul of his sister Dr. Mai A. Tammam who passed away on 19 of March 2022, she was always a kind supporter in all aspects of his life. Amr El-Demerdash is thankful to his home universities, University of East Anglia (UK) and Mansoura University (Egypt) for the unlimited support, inside and outside.

Appendix A. Supplementary data

Supplementary data to this article can be found online at https://doi.org/10.1016/j.fitote.2025.106749.

Data availability

The data presented in this study are available in the present article and the supplementary material.

References

- [1] W. Zhang, X. Guan, X. Qiu, T. Gao, W. Yu, M. Zhang, L. Song, D. Liu, J. Dong, Z.J.A. S.S. Jiang, Bioactive composite Janus nanofibrous membranes loading Ciprofloxacin and Astaxanthin for enhanced healing of full-thickness skin defect wounds 610 (2023) 155290.
- [2] S. Wei, P. Xu, Z. Yao, X. Cui, X. Lei, L. Li, Y. Dong, W. Zhu, R. Guo, B.J. Cheng, A composite hydrogel with co-delivery of antimicrobial peptides and platelet-rich plasma to enhance healing of infected wounds in diabetes 124 (2021) 205–218.
- [3] X. Ding, G. Li, P. Zhang, E. Jin, C. Xiao, X.J.A.F.M. Chen, Injectable self-healing hydrogel wound dressing with cysteine-specific on-demand dissolution property based on tandem dynamic covalent bonds 31 (2021) 2011230.
- [4] O. Catanzano, F. Quaglia, J.S. Boateng, Wound dressings as growth factor delivery platforms for chronic wound healing 18 (2021) 737–759.
- [5] M.G. El Baassiri, L. Dosh, H. Haidar, A. Gerges, S. Baassiri, A. Leone, F. Rappa, A.J. B. Jurjus, Nerve growth factor and burn wound healing: Update of molecular interactions with skin cells 49 (2023) 989–1002.
- [6] R. Augustine, A. Hasan, Y.B. Dalvi, S.R.U. Rehman, R. Varghese, R.N. Unni, H. C. Yalcin, R. Alfkey, S. Thomas, A.-E.J.M.S. Al Moustafa, Growth factor loaded in situ photocrosslinkable poly (3-hydroxybutyrate-co-3-hydroxyvalerate)/gelatin methacryloyl hybrid patch for diabetic wound healing 118 (2021) 111519.
- [7] P. Jewo, I. Fadeyibi, O. Babalola, L. Saalu, A. Benebo, M. Izegbu, O. Ashiru, F. Disasters, A comparative study of the wound healing properties of moist exposed burn ointment (MEBO) and silver sulphadiazine 22 (2009) 79.
- [8] O. Hlokoane, M.J.S.P.J. Sello, Antimicrobial wound healing properties of indigenous medicinal plants of Lesotho and the pharmacist's role in minor wound care 88 (2021), 33a-33e.
- [9] P. Monika, M.N. Chandraprabha, A. Rangarajan, P.V. Waiker, K.N. Chidambara Murthy, Challenges in healing wound: role of complementary and alternative medicine 8 (2022) 791899.
- [10] A.G. Atanasov, S.B. Zotchev, V.M. Dirsch, C.T. Supuran, Natural products in drug discovery: advances and opportunities 20 (2021) 200–216.
- [11] R. Marahatha, K. Gyawali, K. Sharma, N. Gyawali, P. Tandan, A. Adhikari, G. Timilsina, S. Bhattarai, G. Lamichhane, A.J.P.R. Acharya, Pharmacologic activities of phytosteroids in inflammatory diseases: mechanism of action and therapeutic potentials 35 (2021) 5103–5124.
- [12] C. Egbuna, S. Kumar, J.C. Ifemeje, S.M. Ezzat, S. Kaliyaperumal, Phytochemicals as Lead Compounds for New Drug Discovery, Elsevier, 2019.
- [13] C. Boston, N. Wong, T. Ganga, K. Chandradatt, J. Rosales, J. Singh, R.J. Kurup, A. M. Research, Comparison and effectiveness of complementary and alternative medicine as against conventional medicine in the treatment and management of Type 2 diabetes 7 (2019) 1–8.
- [14] F. Miao, Y. Li, Z. Tai, Y. Zhang, Y. Gao, M. Hu, Q.J. Zhu, Antimicrobial peptides: the promising therapeutics for cutaneous wound healing 21 (2021) 2100103.
- [15] N. Mayet, Y.E. Choonara, P. Kumar, L.K. Tomar, C. Tyagi, L.C. Du Toit, V.J. Pillay, A comprehensive review of advanced biopolymeric wound healing systems 103 (2014) 2211–2230.
- [16] A.E. Stoica, A.M. Grumezescu, A.O. Hermenean, E. Andronescu, B.S.J.N. Vasile, Scar-free healing: current concepts and future perspectives 10 (2020) 2179.
- [17] F. Wang, Y. Gao, H. Li, L. Zhou, H. Shi, S. Feng, J. Chen, Z.J.N.R. Mei, Effect of natural-based biological hydrogels combined with growth factors on skin wound healing 11 (2022) 2493–2512.
- [18] P.-H. Wang, B.-S. Huang, H.-C. Horng, C.-C. Yeh, Y.-J. Chen, Wound healing 81 (2018) 94–101.
- [19] S.A. Guo, L.A. Di Pietro, Factors affecting wound healing 89 (2010) 219–229.
- [20] M. Olsson, K. Järbrink, U. Divakar, R. Bajpai, Z. Upton, A. Schmidtchen, J.J. Car, The humanistic and economic burden of chronic wounds: a systematic review 27 (2019) 114–125.
- [21] E. Öhnstedt, H. Lofton Tomenius, E. Vågesjö, M.J. Phillipson, The discovery and development of topical medicines for wound healing 14 (2019) 485–497.
- [22] S.-L. Chen, H. Yu, H.-M. Luo, Q. Wu, C.-F. Li, A. Steinmetz, Conservation and sustainable use of medicinal plants: problems, progress, and prospects 11 (2016) 1–10
- [23] N. Singh, R. Pandey, S.K. Chandraker, S. Pandey, S. Malik, D. Patel, Use of wild edible plants can meet the needs of future generation, in: Agro-biodiversity and Agri-ecosystem Management, Springer, 2022, pp. 341–366.
- [24] S.K. Uniyal, K. Singh, P. Jamwal, B.J. Lal, Traditional use of medicinal plants among the tribal communities of Chhota Bhangal, Western Himalaya 2 (2006) 1–8.
- [25] A. Thakur, S. Singh, K. Dulta, N. Singh, B. Ali, A. Hafeez, D.C. Vodnar, R.A. Marc, Nutritional evaluation, phytochemical makeup, antibacterial and antioxidant properties of wild plants utilized as food by the Gaddis-a tribal tribe in the Western Himalayas 4 (2022) 1010309.

- [26] A. Singh, P.J. Singh, An ethnobotanical study of medicinal plants in Chandauli District of Uttar Pradesh, India 121 (2009) 324–329.
- [27] A. Singh, N. Singh, S. Singh, R.P. Srivastava, L. Singh, P.C. Verma, H.P. Devkota, L. U. Rahman, B. Kumar Rajak, A.J. Singh, The industrially important genus Kaempferia: an ethnopharmacological review 14 (2023) 1099523.
- [28] P. Sharma, R. Manchanda, R. Goswami, S.J.E.C. Chawla, S. Sustainable Development: Volume 2: biodiversity, W. Management, Biodiversity and therapeutic potential of medicinal plants, (2020) 27–44.
- [29] N.J.M.G.C. Morsy, Phytochemical analysis of biologically active constituents of medicinal plants 13 (2014) 7–21.
- [30] R. Yadav, M.J. Agarwala, Phytochemical analysis of some medicinal plants 3 (2011)
- [31] N. Sahu, N. Singh, K.R. Arya, S.S. Reddy, A.K. Rai, V. Shukla, J. Pandey, T. Narender, A.K. Tamrakar, B.J. Kumar, Assessment of the dual role of Lyonia ovalifolia (Wall.) Drude in inhibiting AGEs and enhancing GLUT4 translocation through LC-ESI-QTOF-MS/MS determination and in silico studies 14 (2023) 1073327
- [32] M. Kumar, R. Mehra, R. Yogi, N. Singh, R.K. Salar, G. Saxena, S.J. Rustagi, A novel tannase from *Klebsiella pneumoniae* KP715242 reduces haze and improves the quality of fruit juice and beverages through detannification 7 (2023) 1173611.
- [33] N.U. Rehman, J.N. Alsabahi, N. Bakht, A. Khan, A.J. Al-Harrasi, Chemical constituents and biological activities of the oil from *Lycium shawii* STEM 56 (2020) 1156–1158.
- [34] W.H. Hassan, H.J. Abdallah, M. Research, UPLC-PDA-ESI-MS/MS analysis, isolation of chemical constituents, cytotoxic, antioxidant, antiviral and antimicrobial activities of the aerial parts of Lycium shawii roem. & schult, (2017).
- [35] S.S. Ali, N.A. El-Zawawy, R. Al-Tohamy, S. El-Sapagh, A.M. Mustafa, J.J. Sun, Lycium shawii Roem. & Schult.: A new bioactive antimicrobial and antioxidant agent to combat multi-drug/pan-drug resistant pathogens of wound burn infections 10 (2020) 13–25.
- [36] N. Kaur, R. Kumar, S. Alhan, H. Sharma, N. Singh, R. Yogi, V. Chhokar, V. Beniwal, M.K. Ghosh, S.K.J.I.C.C. Chandraker, *Lycium shawii* mediated green synthesis of silver nanoparticles, characterization and assessments of their phytochemical, antioxidant, antimicrobial properties 159 (2024) 111735.
- [37] H. Sher, M.N. Alyemeni, Evaluation of anti-diabetic activity and toxic potential of Lycium shawii in animal models 5 (2011) 3387–3395.
- [38] R. Yao, M. Heinrich, C.S. Weckerle, The genus Lycium as food and medicine: A botanical, ethnobotanical and historical review 212 (2018) 50–66.
- [39] A. Gaweesh, A. Sengab, H. Osman, A.J.M.A.P. Abdou, Phytoconstituents, cytotoxic, antioxidant and hepatoprotective activities of the aerial parts of *Lycium shawii* R. growing in Egypt 4 (2015) 1–7.
- [40] M. Suleiman, N. Bhat, S. Jacob, R.J. Thomas, Germination Studies in Lycium shawii Roem. and Schult vol. 7, 2011, pp. 26–28.
- [41] A. Tahraoui, J. El-Hilaly, Z. Israili, B.J. Lyoussi, Ethnopharmacological survey of plants used in the traditional treatment of hypertension and diabetes in southeastern Morocco (Errachidia province) 110 (2007) 105–117.
- [42] E. Abdel-Sattar, F.M. Harraz, S.M. Al-Ansari, S. El-Mekkawy, C. Ichino, H. Kiyohara, K. Otoguro, S. Omura, H.J. Yamada, Antiplasmodial and antitrypanosomal activity of plants from the kingdom of Saudi Arabia 63 (2009) 232–239
- [43] T.A. Ahmed, H.J. Al Naemi, Biological activities of Lycium shawii leaves extract 3 (2010) 697–700.
- [44] C.P. Palanisamy, P. Alugoju, S. Jayaraman, S.J.F. Poompradub, Nigella sativa L. seed extracts promote wound healing progress by activating VEGF and PDGF signaling pathways: an in vitro and in silico study 12 (2023).
- [45] P. Bao, A. Kodra, M. Tomic-Canic, M.S. Golinko, H.P. Ehrlich, H.J. Brem, The role of vascular endothelial growth factor in wound healing 153 (2009) 347–358.
- [46] A.H. El-Banna, F.S. Youssef, H. Youssef Elzorba, A.M. Soliman, G.G. Mohamed, S. H. Ismail, M.R. Mousa, H.A. Elbanna, A.S. Osman, Evaluation of the wound healing effect of neomycin-silver nano-composite gel in rats 36 (2022), 03946320221113486.
- [47] S.A. Alsareii, N.A. Alzerwi, M.Y. Alasmari, A.M. Alamri, M.H. Mahnashi, I. A. Shaikh, C. Savant, P.V. Kulkarni, A.K. Shettar, J.H. Hoskeri, L. Manilkara Zapota, Extract topical ointment application to skin wounds in rats speeds up the healing process 14 (2023) 1206438.
- [48] R.H. Mekky, E. Abdel-Sattar, M.-H. Abdulla, A. Segura-Carretero, K. Al-Khayal, W. M. Eldehna, M.J. del Mar Contreras, Metabolic profiling and antioxidant activity of fenugreek seeds cultivars 'Giza 2' and 'Giza 30' compared to other geographically-related seeds 24 (2024) 101819.
- [49] N.M. Saeed, L.A. Ramadan, W.A. El-Sabbagh, M.A. Said, H.M. Abdel-Rahman, R.H. J.F. Mekky, Exploring the anti-osteoporosis potential of *Petroselinum crispum* (Mill.) Fuss extract employing experimentally ovariectomized rat model and network pharmacology approach 175 (2024) 105971.
- [50] S.H. Sweilam, M.S. Abd El Hafeez, M.A. Mansour, R.H.J.P. Mekky, Unravelling the phytochemical composition and antioxidant potential of different parts of *Rumex* vesicarius L.: A RP-HPLC-MS-MS/MS, Chemometrics, and molecular docking-based comparative study 13 (2024) 1815.
- [51] A. Tej, R.H. Mekky, M. del Mar Contreras, A. Feriani, M. Tir, B. L'taief, M. O. Alshaharni, B. Faidi, K. Mnafgui, Z.J.F.B. Abbes, Eucalyptus torquata seeds: Investigation of phytochemicals profile via LC-MS and its potential cardiopreventive capacity in rats 59 (2024) 103666.
- [52] A.S. El-Demerdash, S.A. Kamel, E.Y. Elariny, H. Henidi, Y. Mahran, H. Alahdal, A. M. Saleh, R.A. Ibrahim, Natural inhibitors of Salmonella MDR efflux pumps AcrAB and AcrD: an integrated in silico, molecular, and in vitro investigation, Int. J. Mol. Sci. 25 (2024) 12949.

- [53] A.S. El-Demerdash, R. Alfaraj, F.A. Farid, M.H. Yassin, A.M. Saleh, G.E. Dawwam, Essential oils as capsule disruptors: enhancing antibiotic efficacy against multidrug-resistant Klebsiella pneumoniae, Front. Microbiol. 15 (2024) 1467460.
- [54] Y. Myung, A.G. de Sá, D.B. Ascher, Deep-PK: deep learning for small molecule pharmacokinetic and toxicity prediction 52 (2024) W469–W475.
- [55] S. Adjei, I.K. Amponsah, E. Ekuadzi, C. Hamilton, J. Gavrilovic, O. Dillon, A. El-Demerdash, E.J.N.P.C. Asante-Kwatia, Assessment of wound healing properties of medicinal plants: The case of Berlinia confusa 20 (2025), 1934578X241311978.
- [56] H. Zhao, K. Bojanowski, Dermatologic uses and effects of Lycium barbarum, in: Lycium Barbarum and Human Health, Springer, 2015, pp. 79–84.
- [57] F. Gong, Z. Wang, Y. Zhang, H. Zhang, J. Gao, X. Li, S. Cheng, G. Ma, F.J. Zhao, Application of *Lycium barbarum* polysaccharide liposome nanoparticles to improve the slow healing of refractory wounds in diabetic foot 20 (2024) 1004–1010.
- [58] S.-E. Byambasuren, J. Wang, G.J. Gaudel, Medicinal value of wolfberry (Lycium barbarum L.) 7 (2019) 90–97.
- [59] B.K. Utpal, B. Sutradhar, M. Zehravi, S.H. Sweilam, U.P. Panigrahy, D. Urs, A. F. Fatima, P.K. Nallasivan, G.S. Chhabra, M.J. Sayeed, Polyphenols in wound healing: unlocking prospects with clinical applications, 2024, pp. 1–27.
- [60] N. Zulkefli, C.N.M. Che Zahari, N.H. Sayuti, A.A. Kamarudin, N. Saad, H. S. Hamezah, H. Bunawan, S.N. Baharum, A. Mediani, Q.U. Ahmed, Flavonoids as potential wound-healing molecules: emphasis on pathways perspective 24 (2023) 4607
- [61] G. Jagetia, K.J.C.D.D. Rao, Hesperidin, a citrus bioflavonoid potentiates repair and regeneration of deep dermal excision wounds of mice whole body exposed to different doses of 60 Co γ-radiation 3 (2018) 000147.
- [62] L. Morbidelli, S. Genah, F.J. Cialdai, Effect of microgravity on endothelial cell function, angiogenesis, and vessel remodeling during wound healing 9 (2021) 720001
- [63] G. Badr, W.N. Hozzein, B.M. Badr, A. Al Ghamdi, H.M. Saad Eldien, O.J. Garraud, Bee venom accelerates wound healing in diabetic mice by suppressing activating transcription factor-3 (ATF-3) and inducible nitric oxide synthase (iNOS)-mediated oxidative stress and recruiting bone marrow-derived endothelial progenitor cells 231 (2016) 2159–2171.
- [64] R. Shi, Y. Jin, C. Cao, S. Han, X. Shao, L. Meng, J. Cheng, M. Zhang, J. Zheng, J. J. Xu, Therapy, Localization of human adipose-derived stem cells and their effect in repair of diabetic foot ulcers in rats 7 (2016) 1–13.
- [65] R.H. Mekky, E. Abdel-Sattar, A. Segura-Carretero, M. Contreras, A comparative study on the metabolites profiling of linseed cakes from Egyptian cultivars and antioxidant activity applying mass spectrometry-based analysis and chemometrics, Food Chem. 395 (2022) 133524.
- [66] S.O. Hassanin, A.M.M. Hegab, R.H. Mekky, M.A. Said, M.G. Khalil, A.A. Hamza, A. Amin, Combining in vitro, in vivo, and network pharmacology assays to identify

- targets and molecular mechanisms of Spirulina-derived biomolecules against breast cancer, Mar. Drugs 22 (2024) 328.
- [67] KNApSAcK-Core-System. http://www.knapsackfamily.com/knapsack_jsp/top.htm l, 2025.
- [68] Reaxys. http://www.reaxys.com, 2025.
- [69] Y.-P. Huang, Z. Xia, W. Xu, T.-Q. Xu, H.-X. Zhang, G.-X. Zhou, Lyciiterpenoids A-D, four new rearranged eudesmane sesquiterpenoids from Lycii cortex, Nat. Prod. Res. 35 (2021) 3625–3633.
- [70] S. Wen, Y. Xu, C. Niu, Q. Liu, L. Zhang, Y. Xiang, W. Wang, Z. Sun, Chemical constituents of the fruits of *Lycium barbarum* and their neuroprotective activity, Chem. Nat. Compd. 56 (2020) 923–926.
- [71] D. Zou, X. Li, X. Zhou, B. Luo, M.O. Faruque, S. Hu, J. Chen, X. Hu, The interaction of anti-inflammatory and anti-tumor components in the traditional Chinese medicine Solanum lyratum Thunb, Nat. Prod. Res. 37 (2023) 4239–4243.
- [72] S.-S. Li, Z.-Y. Cheng, Y.-Y. Zhang, R. Guo, X.-B. Wang, X.-X. Huang, L.-Z. Li, S.-J. Song, Sesquiterpenoids from the herbs of *Solanum lyratum* and their cytotoxicity on human hepatoma cells, Fitoterapia 139 (2019) 104411.
- [73] L. Li, J. Qiu, M. Wei, Y. Xie, H. Yu, Y. Guo, Y. Cheng, W. Yao, Inhibition of Candida albicans and induced vaginitis by sapindus water extract, Nat. Prod. Res. 35 (2021) 2987–2991
- [74] N.M. Fayek, R.H. Mekky, C.N. Dias, M. Kropf, A.G. Heiss, L.A. Wessjohann, M. A. Farag, UPLC-MS metabolome-based seed classification of 16 Vicia species: A Prospect for Phyto-equivalency and chemotaxonomy of different accessions, J. Agric. Food Chem. 69 (2021) 5252–5266.
- [75] X. Wang, W. Li, S. Lu, Z. Ma, Modulation of the wound healing through noncoding RNA interplay and GSK-3β/NF-κB signaling, Interaction 2021 (2021) 9709290.
- [76] I.R. Botusan, V.G. Sunkari, O. Savu, A.I. Catrina, J. Grünler, S. Lindberg, T. Pereira, S. Ylä-Herttuala, L. Poellinger, K. Brismar, Stabilization of HIF-1α is critical to improve wound healing in diabetic mice 105 (2008) 19426–19431.
- [77] G. Li, C.-N. Ko, D. Li, C. Yang, W. Wang, G.-J. Yang, C. Di Primo, V.K.W. Wong, Y. Xiang, L. Lin, A small molecule HIF-1α stabilizer that accelerates diabetic wound healing 12 (2021) 3363.
- [78] J.D. Hayes, S. Chowdhry, A.T. Dinkova-Kostova, C.J.B.S.T. Sutherland, Dual regulation of transcription factor Nrf2 by Keap1 and by the combined actions of β-TrCP and GSK-3 43 (2015) 611–620.
- [79] C. Mihai, S. Bao, J.-P. Lai, S.N. Ghadiali, D.L. Knoell, PTEN inhibition improves wound healing in lung epithelia through changes in cellular mechanics that enhance migration 302 (2012) L287–L299.
- [80] S. Rodriguez, U. Huynh-Do, The role of PTEN in tumor angiogenesis 2012 (2012) 141236.

<u>Update</u>

Fitoterapia

Volume 185, Issue , September 2025, Page

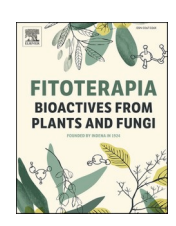
DOI: https://doi.org/10.1016/j.fitote.2025.106791

\$ SUPER

Contents lists available at ScienceDirect

Fitoterapia

journal homepage: www.elsevier.com/locate/fitote





Corrigendum to "Chemical profiling of *Lycium shawii* via RP-HPLC-QTOF-MS and MS/MS: unveiling its *in-vivo* wound-healing potential supported by molecular docking investigations" [Fitoterapia 185 (2025) 106749]

Mahmoud Moustafa ^a, Walaa S. Aboelmaaty ^a, Weaam Ebrahim ^a, Reham Hassan Mekky ^b, Mohamed A. Tammam ^c, Amr El-Demerdash ^{d,e,*}, Ahmed M. Zaghloul ^{a,**}

- ^a Department of Pharmacognosy, Faculty of Pharmacy, Mansoura University, Mansoura 35516, Egypt
- b Department of Pharmacognosy, Faculty of Pharmacy, Egyptian Russian University, Badr City, Cairo-Suez Road, 11829 Cairo, Egypt
- ^c Department of Biochemistry, Faculty of Agriculture, Fayoum University, Fayoum 63514, Egypt
- ^d Department of Chemistry, Faculty of Sciences, Mansoura University, Mansoura 35516, Egypt

The authors regret the need to correct the ethical approval declaration as follows:

Ethical Approval Code: MU-ACUC (PHARM.PHD.24.12.47, approved on 02/01/2025).

The authors would like to apologize for any inconvenience caused.

We hope this detailed explanation addresses all concerns raised. We take these matters very seriously and reaffirm that our study was conducted in full compliance with the ethical policies set forth by both our institution and Fitoterapia. The authors would like to apologize for any inconvenience caused.

E-mail addresses: a_eldemerdash83@mans.edu.eg, A.Eldemerdash@uea.ac.uk (A. El-Demerdash), amzaghloul@yahoo.com (A.M. Zaghloul).

e School of Chemistry, Pharmacy and Pharmacology, University of East Anglia, Norwich Research Park, Norwich NR4 7TJ, United Kingdom

DOI of original article: https://doi.org/10.1016/j.fitote.2025.106749.

^{*} Corresponding author at: Department of Chemistry, Faculty of Sciences, Mansoura University, Mansoura 35516, Egypt.

^{**} Corresponding author.